We are IntechOpen, the world's leading publisher of Open Access books Built by scientists, for scientists

4,800
Open access books available

122,000
International authors and editors

135M
Downloads

Our authors are among the

154
Countries delivered to

TOP 1%
most cited scientists

12.2%
Contributors from top 500 universities

BOOK CITATION INDEX
CLARIVATE ANALYTICS
INDEXED

WEB OF SCIENCE™

Selection of our books indexed in the Book Citation Index
in Web of Science™ Core Collection (BKCI)

Interested in publishing with us?
Contact book.department@intechopen.com

Numbers displayed above are based on latest data collected.
For more information visit www.intechopen.com

Organic-Inorganic Hybrid Coatings for Corrosion Protection of Metallic Surfaces

Samarah V. Harb, Andressa Trentin,
Ruben F. O. Torrico, Sandra H. Pulcinelli,
Celso V. Santilli and Peter Hammer

Additional information is available at the end of the chapter

Abstract

A variety of organic-inorganic hybrids have been designed to act as anticorrosive coatings of metallic substrates. Among them, epoxy-silica and poly(methyl methacrylate) (PMMA)- silica hybrids, prepared by the sol-gel process and deposited onto steel or aluminum alloys, have demonstrated high anticorrosive efficiency combined with high thermal and mechanical resistance. Lignin, carbon nanotubes, and graphene oxide have been incorporated into PMMA-silica hybrids as reinforcement agents, and cerium (IV) as corrosion inhibitor. Both hybrids were characterized in terms of their structural and thermal characteristics using different pectroscopies, microscopies and thermogravimetric analysis. Both hybrids present homogeneous nanostructure composed of highly condensed silica nanodomains covalently bonded to the polymeric phase. The transparent coatings with a thickness of 2–7 μm have low surface roughness, high adhesion to metallic substrates, elevated thermal stability, and excellent barrier behavior. Electrochemical impedance spectroscopy showed for coated samples a high corrosion resistance of up to 50 GΩ cm2 and durability >18 months in saline solution. Further improvement of corrosion resistance, thermal and mechanical stability was achieved by incorporation of lignin, carbon nanotubes, and graphene oxide into PMMA-silica matrix, and a self-healing effect was observed after Ce(IV) addition. The results are compared and discussed with those recently reported for a variety of hybrid coatings.

Keywords: organic-inorganic hybrids, anticorrosive coatings, corrosion inhibitors, nanocomposites, self-healing, sol-gel process

1. Introduction

Since the discovery of copper in prehistoric times, an extensive diversity of metallic materials has emerged, as pure metals or metal alloys. Brass, bronze, steel, titanium, and aluminum alloys are currently the most applied metallic materials, notwithstanding the natural tendency to suffer corrosion under aggressive conditions and thus return to their original ore. To overcome issues related with economical losses and lack of safety, occasioned by metal corrosion, several protection methods have been developed, including the use of:

new alloys with higher corrosion resistance, but in addition to the high cost associated with their development, the use of new alloys requires the replacement of the metallic components;

corrosion inhibitors, substances which reduce or even eliminate corrosion, when present in suitable concentrations in the corrosive medium. Inhibition is accomplished by one or a combination of several mechanisms, such as adsorption, forming a ultrathin film with a thickness of only few molecular layers; in form of visible bulky precipitates, which coat the metal surface; or other common methods consisting of the combination of adsorption, conversion, and oxidation processes to form a passive layer. Some examples of most applied inhibitors are phosphates, chromates, silicates, hydroxides, carbonates, sulfates, aldehydes, amines, nitrogen heterocyclic compounds, urea, among others [1];

cathodic protection that uses a sacrificial metal to protect the metallic structure of interest. It is commonly used to prevent corrosion in large port structures, offshore platforms, and pipelines to transport water, oil, and gas;

conversion layer produced by converting the metal surface into a corrosion-resistant form. The main processes include anodizing, phosphatizing, and chromating, and they are frequently used as pretreatment for subsequent overcoats [1]. Anodizing is based on the formation of a protective surface layer, formed by oxides and hydroxides, by application of an external current. In an electrochemical cell, the surface of the metal anode is transformed into an oxide layer of defined thickness, which improves significantly the corrosion resistance and the adhesion of subsequent paints. This method is frequently applied to protect aluminum alloys but can be used also for titanium, zinc, magnesium, and other metal substrates. Besides the presence of microscopic fissures in the anodizing coating that can lead to corrosion, another drawback is the susceptibility of the oxide layer to chemical dissolution in the presence of high- and low-pH environments. Phosphatizing is mostly applied on steel substrates to produce an insoluble and porous phosphate layer that serves as an excellent base for coatings. For instance, car bodies have been phosphatized prior to the application of coatings for many years [1]. Alternatively, surface passivation using chromate conversion coatings has been used especially to protect aluminum alloys in the aerospace industry, for metal fittings and for packaging steel [2, 3]. Such coatings are formed by the reduction of Cr(VI) species to hydrated Cr_2O_3; however, the conversion process as well as the final coating retains a small amount of unreacted Cr(VI), a highly toxic species which can be released to the environment. Recently, increasing efforts are focused on the development of innovative eco-friendly alternatives due to increasingly strict legislation regulations which demand a reduction of hexavalent chromates usage [3];

protective coatings applied on metal surfaces result in a barrier between the metal and the corrosive medium, thus preventing or minimizing the corrosion process.

The use of coatings on metallic surfaces has various advantages, such as relatively low costs, environmental compatibility, and the possibility to apply them on metallic components already in use. Consequently, different kinds of protective coatings have been developed, comprising metallic, inorganic, organic, or organic-inorganic materials. The application of many metal coatings, such as chromium, zinc, nickel, aluminum, and copper, involves usually inherent pollution and toxicity-related problems. The most widely used metallic coating is zinc, commonly deposited on carbon steel by hot-dip on a molten zinc bath, process called galvanization, after which the metal substrate acquires a zinc-rich top layer with a thickness of approximately 10 µm. Inorganic coatings comprise ceramics (silica, titania, zirconia, alumina), glass, carbon, etc [1]. Although the inorganic coatings present higher corrosion resistance compared to bare substrates, they usually exhibit residual porosity and stress-induced cracks, which limit their use as efficient corrosion barrier as they allow the diffusion of corrosive species to the underlying metal [4, 5]. Organic materials such as epoxy, poly(methyl methacrylate) (PMMA), polyurethane (PU), polyesters, fluoropolymers, and related paints, combined with anticorrosive primer containing various types of pigments, are widely applied as protective coatings. This is justified by the simplicity of deposition, their dense and homogeneous structure, and consequently high corrosion resistance in aggressive environments. However, their lack of thermal stability, mechanical resistance and adhesion to metallic surfaces can result in serious restriction of their long-term stability.

Organic-inorganic hybrids stand for a class of materials formed by the combination of a polymeric and a ceramic phase, resulting in a nanocomposite material with unique properties. New functionalities result from the synergy of both components, achieved by a careful adjustment of the nature, proportion, and the type of interaction at the interface of both phases. One of the most used methodologies to produce organic-inorganic hybrid materials is the sol-gel process, which allows due to its versatility to control the structure and the functional properties. Through hydrolysis and condensations reactions, the sol-gel route allows the obtain high purity, homogeneous, and structurally tuneable materials, which have a wide range of applications such as catalysts, drug release systems, photochromic devices, biosensors, transparent insulating films, and anticorrosive coatings with excellent barrier properties [6]. The latter characteristic is related to the possibility to prepare a dense organic-inorganic network structure by linking both phases covalently on the molecular scale, and furthermore, the ability to covalently bond the inorganic phase with metallic substrates, leading to highly adherent coatings. Consequently, intense research efforts are presently focused on the development of organic-inorganic hybrid coatings in form of passive barrier layers with low permeability for corrosive species such as chloride ions, water, and oxygen.

There are various methodologies to investigate the corrosion protection efficiency of coated metals; however, the most applied electrochemical techniques are electrochemical impedance spectroscopy (EIS), potentiodynamic polarization, and chronopotentiometry. Among them, EIS allows for a deeper analysis of the electrolyte/coating/substrate systems, due to the possibility to fit the data using equivalent electrical circuits, which permit to extract important

electrochemical parameters such as coating capacitance, pore resistance, double layer capacitance, charge transfer resistance, water uptake, diffusivity, among others. Additional methods like salt spray test and immersion techniques are used according to different norms for the qualitative and quantitative evaluation of corrosion zones, pitting, and for the determination of corrosion rates. To evaluate the electrochemical performance of the protective system for a given corrosive environment and coating thickness, the most important criteria are (i) the magnitude of the initial impedance modulus obtained by EIS at low frequency, defined as corrosion resistance; (ii) the values of the open circuit potential, obtained by chronopotentiometry; and (iii) the time evolution of both parameters, to evaluate the long-term stability of the coatings. For industrial application, another important aspects have to be considered such as the simplicity of the synthesis process, low costs of reagents, and their environmental compatibility.

One example of an efficient corrosion protection of mild steel was recently reported for a hybrid system combining an epoxy-siloxane topcoat with an epoxy primer containing micaceous iron oxide and zinc phosphate pigments [7]. The electrochemical measurements showed a high-impedance modulus of up to 100 $G\Omega$ cm^2, remaining stable for more than 1 year in contact with 3% NaCl solution. The authors attribute the excellent protection to the high resistance of the coating against water uptake provided by suitable epoxy/primer combination and the relatively high thickness (~140 μm) of this coating system. In another recent study, Ammar et al. [8] report on high-performance hybrid coatings based on acrylic-silica polymeric matrix reinforced by SiO_2 nanoparticles, applied to mild steel with a thickness of 75 μm by brush coating. EIS measurements confirmed the high-corrosion protection efficiency with an impedance modulus of more than 10 $G\Omega$ cm^2, decreasing one decade after 90 days of immersion in 3.5% NaCl solution. Visuet et al. [9] obtained similar results for polyurethane/polysiloxane hybrid coatings containing TiO_2 as pigment. The EIS analysis showed that coatings loaded with 10-wt% TiO_2 (75 μm thick) were able to withstand 263 days, in 3.5% NaCl solution, with almost unaltered corrosion resistance of about 100 $G\Omega$ cm^2. Their model proposes that the TiO_2 pigment works as a charge (ionic) storage surfaces, thus enhancing the barrier property of the coating against electrolyte uptake.

The above results demonstrate that elevated anticorrosive performance is usually achieved for sophisticated barrier coatings with an average thickness in the order of dozens to hundreds micrometers. For the market, however, which aims on economic and efficient solutions, elevated thickness, and complexity of the coating system, implies elevated material costs and weight increase, issues that are hardly to be accepted, especially by the aerospace industry. In this regard, dos Santos and coauthors [10] have successfully prepared highly efficient PMMA-silica coatings having a thickness of only ~2 μm, which were able to withstand aggressive saline/acid (0.05 mol L^{-1} NaCl + 0.05 mol L^{-1} H_2SO_4) and 3.5% NaCl environments for up to 105 and 196 days, respectively, maintaining the corrosion resistance in the $G\Omega$ cm^2 range. The excellent performance of the primer free coating was explained by the high connectivity of reticulated sub-nanometric silica domains densely interconnected by short PMMA chain segments. Another results that confirmed the viability of thin hybrid films as efficient corrosion barrier have been reported in the study of Harb et al. [11]. The authors showed that the addition of cerium (IV) salt into PMMA-silica system results in a further improvement

of the corrosion resistance and durability of the coatings applied to polished carbon steel by dip-coating. The electrochemical behavior of ~1.5 μm thick films reached for a Ce/Si molar ratio of 0.7% an impedance modulus of about 10 GΩ cm^2 (NaCl 3.5% solution) and remained stable within one order of magnitude for 304 days, a performance typically observed for high performance paint systems. The remarkable anticorrosive protection has been associated with the role of Ce(IV) as oxidation agent leading to an enhancement of the overall connectivity of the hybrid network, induced by the enhanced polymerization of organic and inorganic moieties.

In contrast to coating system designed as passive barrier, recent trends aim on the development of active multifunctional anticorrosive coatings with self-healing ability, high-thermal stability, and mechanical resistance, among other functionalities. Inspired by biological systems, the self-healing ability involves the complete recovery of the original properties of the material after suffering macroscopic lesions, induced by mechanical or chemical processes. Various strategies have been used to prepare self-healing coatings, usually containing an active compound, whether stored in microcapsules or incorporated into the coating. They can be activated by temperature increase, UV, pH gradient, breaking of capsules, or changes in the chemical environment [12, 13]. A number of studies report on the use of cerium salts (chloride and nitrates) and ceria nanoparticles as inhibitors, preventing corrosion by the self-healing ability in affected areas of inorganic, organic, and hybrid coatings. The resulting substantial lifetime increase is attributed to the formation of insoluble oxides and hydroxides in the corroded zones [3, 11, 14–17]. On the other hand, significant improvements of thermal and mechanical properties have been achieved by incorporation of clays, lignin, carbon nanotubes, graphene oxide, and graphene into polymeric or organic-inorganic matrices [18–20].

This chapter reports on recent results obtained for high-performance PMMA-silica and epoxy-silica hybrids coatings, correlating their structural properties with the corrosion protection efficiency, accessed by potentiodynamic polarization and electrochemical impedance spectroscopy. Moreover, several interesting finding are presented regarding PMMA-silica hybrids reinforced with lignin, carbon nanotubes, and graphene oxide to improve their thermal and mechanical properties, as well as some recent results on active corrosion inhibition by the self-healing ability of Ce(IV) containing PMMA-silica coatings.

2. Experimental

2.1. Epoxy-silica and PMMA-silica hybrid synthesis

All reagents used to epoxy-silica and PMMA-silica hybrids synthesis were purchased from Sigma-Aldrich and used as received, apart from the methyl methacrylate (MMA) monomer, which had been distilled before use to remove the polymerization inhibitor. The molecular structures of the epoxy-silica and PMMA-silica hybrid precursors are presented in **Figures 1** and **2**, respectively, and the synthesis procedures are summarized in **Figure 3**.
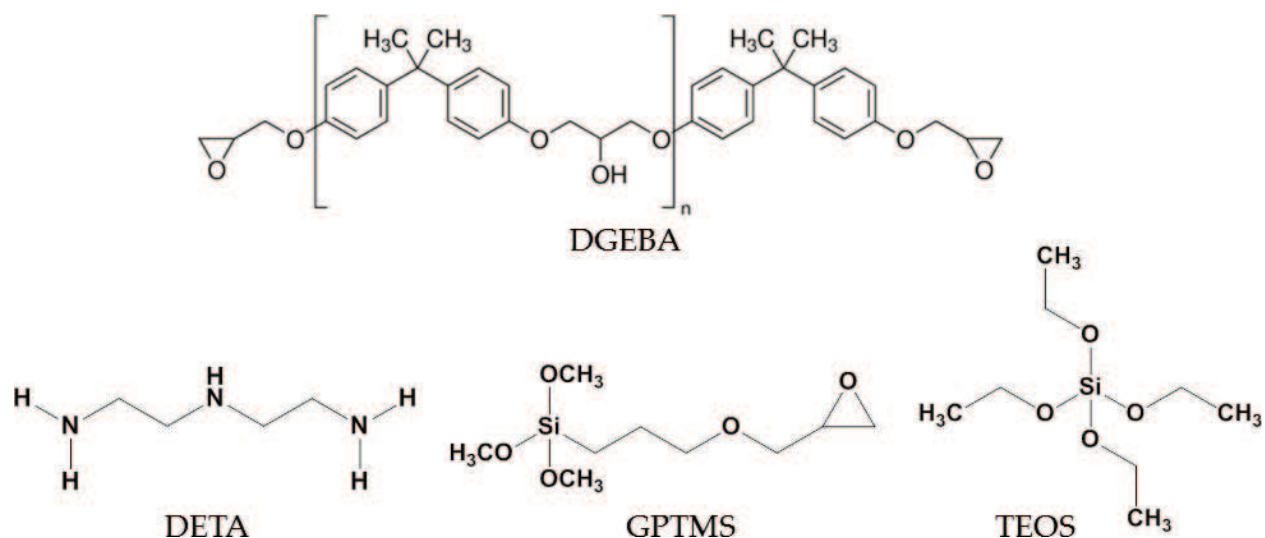
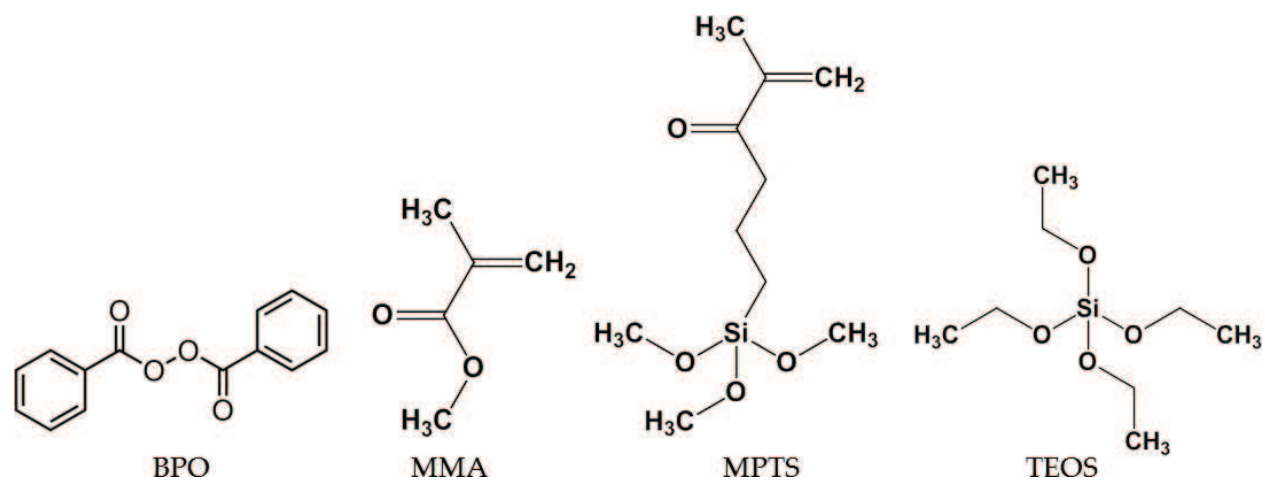**Figure 1.** Molecular structures of the epoxy-silica hybrid precursors.

Figure 2. Molecular structures of the PMMA-silica hybrid precursors.

Epoxy-silica hybrids were prepared from the curing reaction of poly(bisphenol A-co-epichlorohydrin), glycidyl end-capped (DGEBA, Mn = 377 g/mol) with diethyltriamine (DETA) as hardener, and (3-glycidoxypropyl)methyltriethoxysilane (GPTMS), as coupling agent between the organic and inorganic phase, combined with the sol-gel hydrolysis and condensation reactions of tetraethoxysilane (TEOS) and GPTMS. In the first step, DGEBA and GPTMS were mixed with DETA in tetrahydrofuran (THF) solvent during 4 h at 70°C and 25 min at 25°C, under constant stirring in a reflux flask. In the next step, TEOS, ethanol, and acid-ified water (pH 1 using nitric acid) were added to the reflux system at room temperature and stirred for an additional 1 h. At this stage, the sol-gel reactions take place, as shown below, where the alkoxide precursors (TEOS and GPTMS) are hydrolyzed, forming Si–OH groups, Eq. (1), which subsequently condense with an initial alkoxide molecule, Eq. (2), or another Si–OH group, Eq. (3), yielding Si–O–Si bond and eliminating alcohol or water, respectively.
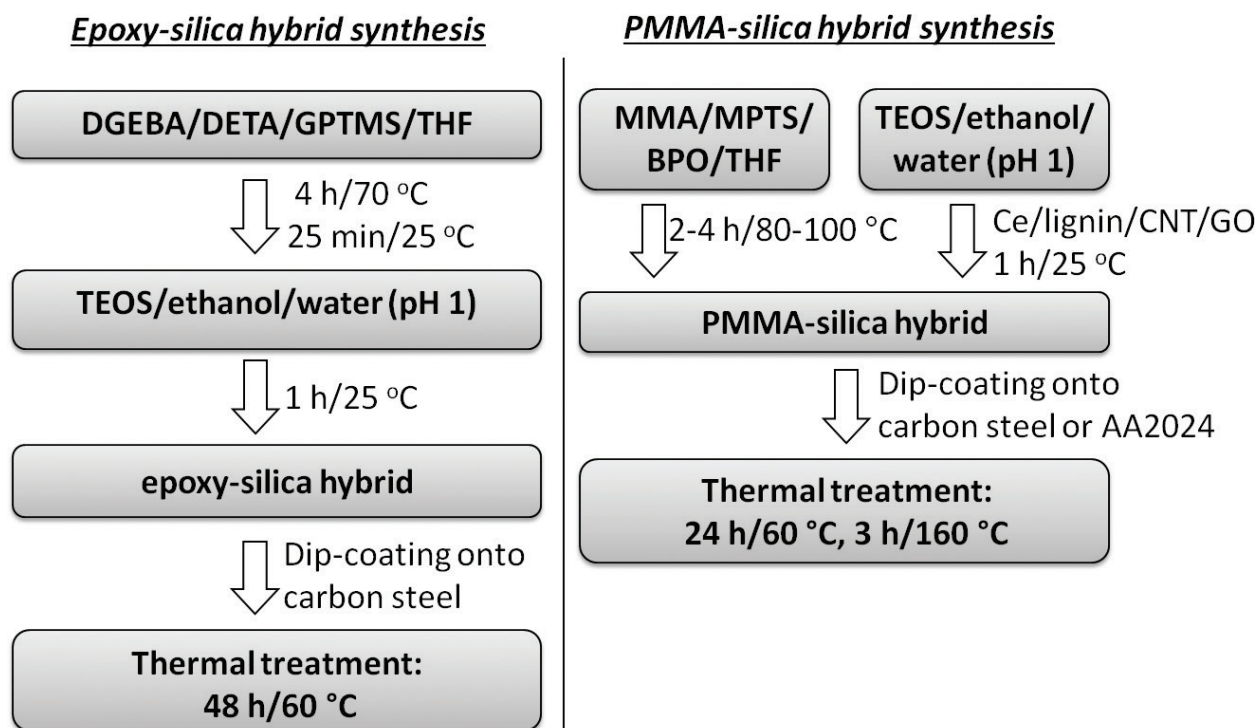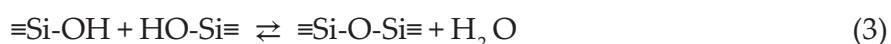
Figure 3. Synthesis procedures used to prepare epoxy-silica and PMMA-silica hybrids.

The homogeneous and transparent sols were used for the film deposition by dip-coating onto A1020 carbon steel.

$$\equiv\text{Si-OR} + \text{H}_2\text{O} \;\rightleftarrows\; \equiv\text{Si-OH} + \text{ROH} \tag{1}$$

$$\equiv\text{Si-OR} + \text{HO-Si}\equiv \;\rightleftarrows\; \equiv\text{Si-O-Si}\equiv + \text{ROH} \tag{2}$$

$$\equiv\text{Si-OH} + \text{HO-Si}\equiv \;\rightleftarrows\; \equiv\text{Si-O-Si}\equiv + \text{H}_2\text{O} \tag{3}$$

Two series of epoxy-silica hybrids were prepared, varying the amount of GPTMS or TEOS and keeping the molar concentrations of other compounds constant (**Figure 4**). In order to ensure a fully cured thermosetting, DETA was added in a proportion that resulted in one oxirane group for each hydrogen atom of the amine groups.

PMMA-silica hybrids have been prepared by the radical polymerization of methyl meth-acrylate (MMA) and 3-(trimethoxysilyl)propyl methacrylate (MPTS, also known as TMSM) using benzoyl peroxide (BPO), as thermal initiator of the polymerization, and tetrahydrofu-ran (THF) as solvent. The sol-gel route has been used to perform the hydrolytic condensation of tetraethoxysilane (TEOS) and MPTS, using ethanol and acidified water (pH 1 using nitric acid), during 1 h at room temperature. In the presence of acidified water, alkoxide precursors (TEOS and MPTS) are hydrolyzed and subsequently condensed to form Si–O–Si bonds. After mixing the organic and inorganic precursor, the obtained transparent and homogeneous sols were used to deposit few micrometer thick films onto A1020 carbon steel or AA2024 alumi-num alloy substrates.
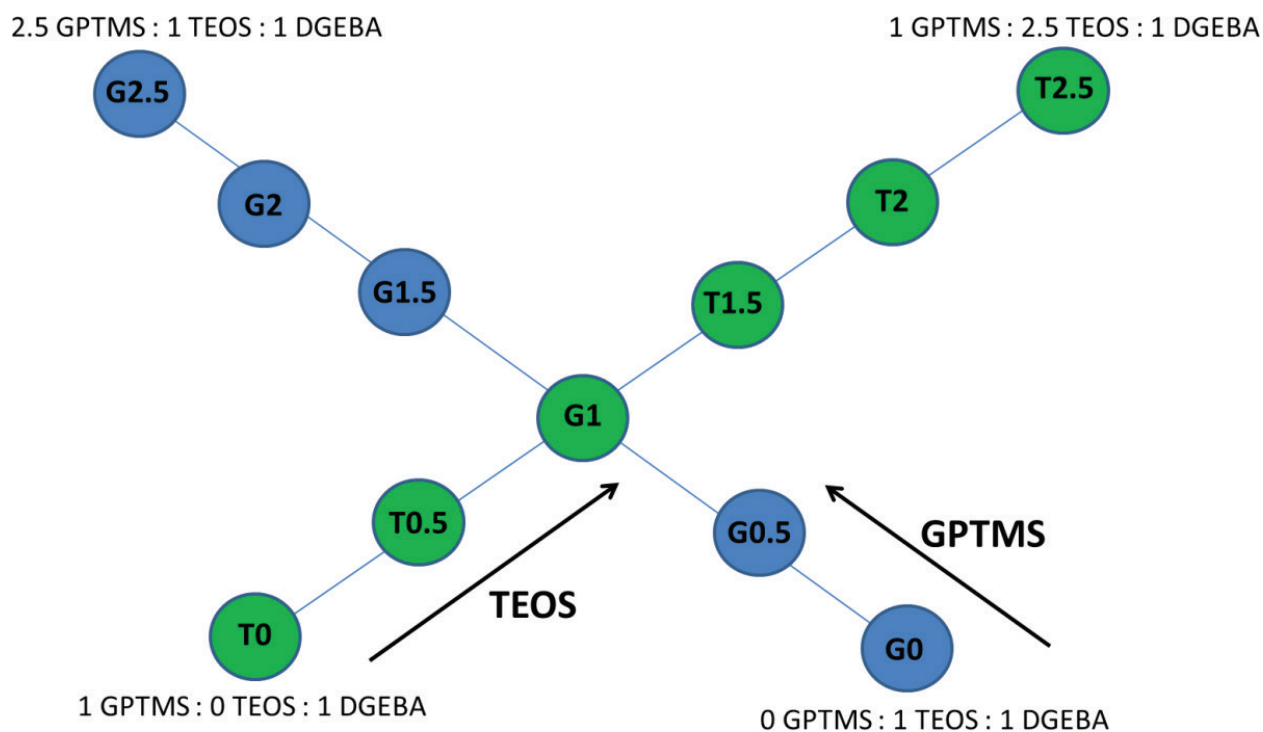
Figure 4. Epoxy-silica hybrids sample names and compositions.

To investigate the relation between structure and barrier properties, the hybrids films were prepared at different synthesis conditions (**Table 1**), varying the ratio between the organic to inorganic phase (MMA/TEOS), the temperature (80–100°C) and time (2–4 h) of the organic precursor reaction, as well as the BPO/MMA molar ratio (0.01–0.1). The molar ratios of H_2O/ $Si = 3.5$ and ethanol/$H_2O = 0.5$ were kept constant. Ce(IV) salt (ammonium cerium nitrate), lignin, carbon nanotube (CNT), and graphene oxide (GO) were added separately as modifier to the inorganic precursor of the PMMA-silica hybrid.

Carbon steel 1020 (25 mm × 20 mm × 5 mm), a ferrous alloy with low carbon content, and 2024 aluminum alloy (20 mm × 20 mm × 1 mm) have been used as substrates. Low-carbon steels are produced in large quantities at relatively low costs and widely used in automobilist, construction, oil industries, etc [21]. Although the use of ferrous alloys is economically viable due to the low cost and versatility, corrosion is the great obstacle when it comes to the durability of these materials that undergo severe corrosion in contact with humid environments, low amounts of chloride ions and acid solutions in general. The 2000 and 7000 series of aluminum alloys, containing roughly 4.3–4.5% copper, 0.5–0.6% manganese, 1.3–1.5% magnesium, are widely used in the aerospace industry due to their improved mechanical properties; however, they are susceptible to enhanced corrosion especially at the grain boundaries. Prior to deposition, all substrates had been sanded with 100, 300, 600, and 1500 grit emery paper, washed with isopropanol for 10 min in an ultrasound bath and dried under a nitrogen stream. The deposition of the hybrids coatings was performed by dip-coating (Microchemistry—MQCTL2000MP) at a rate of 14 cm min⁻¹, with 1 min of immersion and air-drying during 10 min at room temperature. This procedure was performed three times for each sample. The coated substrates and

Samples	MMA:MPTS:TEOS molar ratio	BPO/MMA molar ratio	Organic phase synthesis	Filler	Reference
M2	2:1:2	0.01	70°C/2 h	–	[22]
M4	4:1:2	0.01	70°C/2 h	–	[22]
M8	8:1:2	0.01	70°C/2 h	–	[22]
M10	10:1:2	0.01	70°C/2 h	–	[22]
M8_4h	8:1:2	0.01	80°C/4 h	–	[18]
M8_4h_E0.2	8:1:2	0.01	80°C/4 h		[10]
M8_T80B0.01	8:1:2	0.01	80°C/4 h	–	–
M8_T90	8:1:2	0.01	90°C/4 h	–	–
M8_T100	8:1:2	0.01	100°C/4 h	–	–
M8_B0.05	8:1:2	0.05	80°C/4 h	–	–
M8_B0.10	8:1:2	0.10	80°C/4 h	–	–
M8_Ce	8:1:2	0.01	70°C/2 h	Ce/Si molar ratio: 0.1, 0.2, 0.3, 0.5, 0.7, 1, 3, 5%	[11]
M8_lignin	8:1:2	0.01	70°C/2 h	lignin: 0.05, 0.10, 0.50, 1.00 wt.%	[20]
M8_CNT	8:1:2	0.01 and 0.05	80°C/4 h	C_{CNT}/Si molar ratio: 0.05%	[18]
M8_GO	8:1:2	0.01 and 0.05	80°C/4 h	C_{GO}/Si molar ratio: 0.05%	[18]

Table 1. PMMA-silica hybrid preparation conditions.

the remaining solution, placed in Teflon holders, were cured for 24 h at 60°C and then 3 h at 160°C to ensure the liberation of all volatile species and the densification of the hybrid matrix.

2.2. Characterization techniques

Structural and morphological characteristics have been investigated using nuclear magnetic resonance spectroscopy (NMR), X-ray photoelectron spectroscopy (XPS), small angle X-ray scattering (SAXS), atomic force microscopy (AFM) and thermogravimetric analysis (TGA). The anticorrosive properties of coated samples were evaluated by exposure of the coated samples to standard 3.5% saline and saline/acid solutions, using electrochemical impedance spectroscopy (EIS).

The thickness of the coatings was determined using a Filmetrics F3-CS optical interference system. An Agilent Technologies Model 5500 atomic force microscope was used to obtain AFM topography images, in tapping mode, with 1×1 µm, of the hybrid coatings deposited on the metallic substrates. ^{29}Si nuclear magnetic resonance spectroscopy (^{29}Si-NMR) measurements of the hybrid powders were performed in a 300-MHz Varian Inova spectrometer, using a Larmor frequency of 59.59 Hz and tetramethyl silane (TMS) as an external standard. The

CasaXPS processing software was used for spectral deconvolution using Gauss profiles. XPS was carried out in a UNI-SPECS UHV surface analysis system, using the Mg Kα radiation (hν = 1253.6 eV) and pass energy of 10 eV to record the high-resolution spectra. The near surface composition was determined from relative peak intensities of carbon (C 1s), oxygen (O 1s) and silicon (Si 2p) corrected by Scofield's atomic sensitivity factor of the corresponding elements. To study the oxidation state of Ce (Ce 3d) and the local bonding structure of carbon (C 1s), oxygen (O 1s), and silicon (Si 2p) of the coatings, the spectra were deconvoluted applying Voigt profiles and Shirley's background subtraction using the CasaXPS software. SAXS experiments were carried out at the SAXS-1 beamline in the National Synchrotron Light Laboratory (LNLS, Campinas, Brazil) to determine the nanostructural characteristics of the hybrids. The scattering intensity I(q) was recorded as a function of the modulus of the scattering wave vector q = ($4\pi/\lambda$) sin θ, θ being half of the scattering angle. The SAXS beamline uses a monochromatic X-ray beam (λ = 1.548 Å) and a 2D detector, Dectris Pilatus 300k, positioned 0.9 m away from the sample holder. Thermogravimetric analysis of unsupported hybrids films was performed in a TA Instruments STD Q600 analyzer, under a nitrogen flow of 100 mL min^{-1}.

The anticorrosive performance of hybrid coatings, deposited on A1020 carbon steel or Al2024 aluminum alloy, was investigated by electrochemical impedance spectroscopy (EIS) with a Gamry Potentiostat Reference 600, using 10 points per decade and RMS amplitude of 10 mV in a frequency range of 50 mHz–100 kHz. The electrochemical cell consisted of an Ag|AgCl|KClsat reference electrode, a platinum mesh counter electrode, a platinum electrode connected to the reference electrode through a 0.1-μF capacitor and the working electrode of either coated or uncoated metal substrate. The measurements were performed once a week, in saline (3.5% NaCl) or saline/acid solutions (0.05-mol L^{-1} H$_2$SO$_4$ + 0.05-mol L^{-1} NaCl), until a significant drop of the impedance modulus was observed, indicating the failure of the coating.

3. Results and discussion

A number of interesting results have been obtained for novel epoxy-silica and PMMA-silica hybrid coatings, concerning their nanostructural properties, modified by the variation of synthesis conditions or by addition of nanofillers, in form of lignin, carbon nanotubes, and graphene oxide. The main purpose of this work was to relate these properties with the barrier characteristics, in terms of corrosion resistance and durability in aggressive environments and to compare the obtained results with those reported for a variety of hybrid coating systems. For the fine tuning of the performance of both coating systems toward an efficient and stable anticorrosive barrier, it is crucial to obtain detailed information on the formation process of the hybrid network and the structural and compositional properties of the nanocomposites.

3.1. Epoxy-silica hybrid

Bisphenol stands for a group of chemical compounds with two hydroxyphenyl functionalities. There is a wide diversity of bisphenol molecules; however, the most common are

the Bisphenol A (BPA) and the Bisphenol F (BPF) (**Figure 5**). Epoxy resins can be produced from the combination of bisphenol, such as bisphenol A, with epichlorohydrin (IUPAC name: 2-(chloromethyl)oxirane)) to give, for example, bisphenol A diglycidyl ether (**Figure 6**). The epoxy resins present in general poor thermal, mechanical, and chemical stability, properties which are however significantly improved when a curing agent is added. Most curing agents are composed of nitrogen-containing molecules that have a functionality equal or superior of three ($f \geq 3$), which provides cross-linking between the bisphenol segments. The functionality is the number of available bonding sites, such as $f = 4$ for diamino diphenyl methane (4 hydrogens prone to provide bond), $f = 6$ for triethylene tetraamine, and $f = 5$ for diethylenetriamine (**Figure 7**). Curing reactions by DETA proceed by S_N2 nucleophilic attack of the curing agent to the less-substituted carbon in the oxirane ring, resulting in its opening and formation of an OH group. The nitrogen of the amine group can attack another epoxy ring resulting in a highly branched polymer system, known as a thermoset, which presents high thermal stability and mechanical resistance [23]. This second nucleophilic attack of nitrogen can occur at the epoxy group of the resin or another molecule containing epoxy group, such
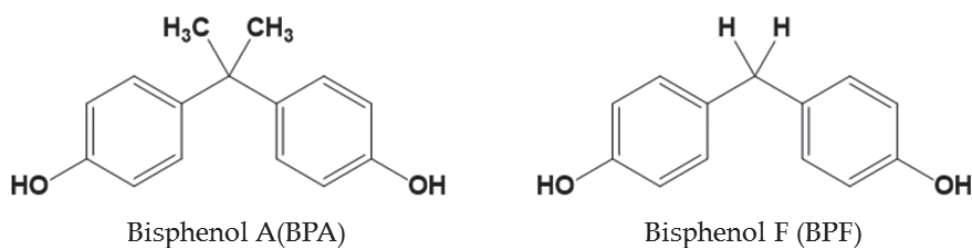

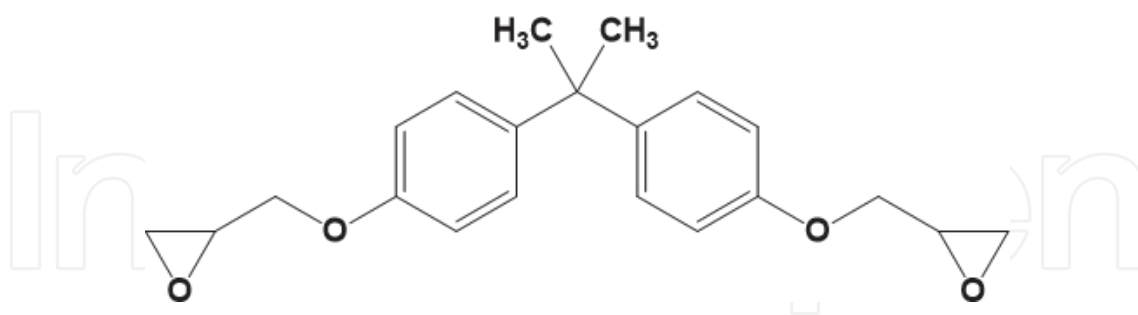**Figure 5.** Common epoxy resin precursors.

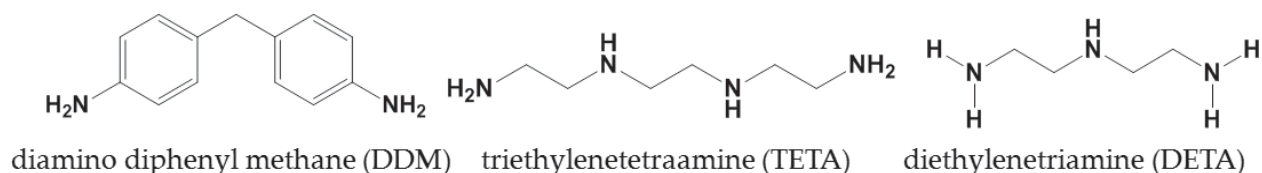**Figure 6.** Bisphenol A diglycidyl ether.

Figure 7. Common curing agents.

as (3-glycidoxypropyl)trimethoxysilane (GPTMS) to produce an organic-inorganic hybrid structure (**Figure 8**).

Simultaneously to the curing reaction, the sol-gel reactions of hydrolysis and condensation take place to produce the silica inorganic phase. GPTMS and TEOS Si–O–R groups, in presence of acidified water, become Si–OH through the hydrolysis reaction, and posteriorly, the Si–OH groups can condense with another Si–OH group or an initial Si–O–R group, forming Si–O–Si bonding and eliminating water or alcohol, respectively.

The surface characterization of the epoxy-silica hybrids deposited on carbon steel has shown that the coatings are uniform, transparent, smooth, and crack free (**Figure 9**). AFM images
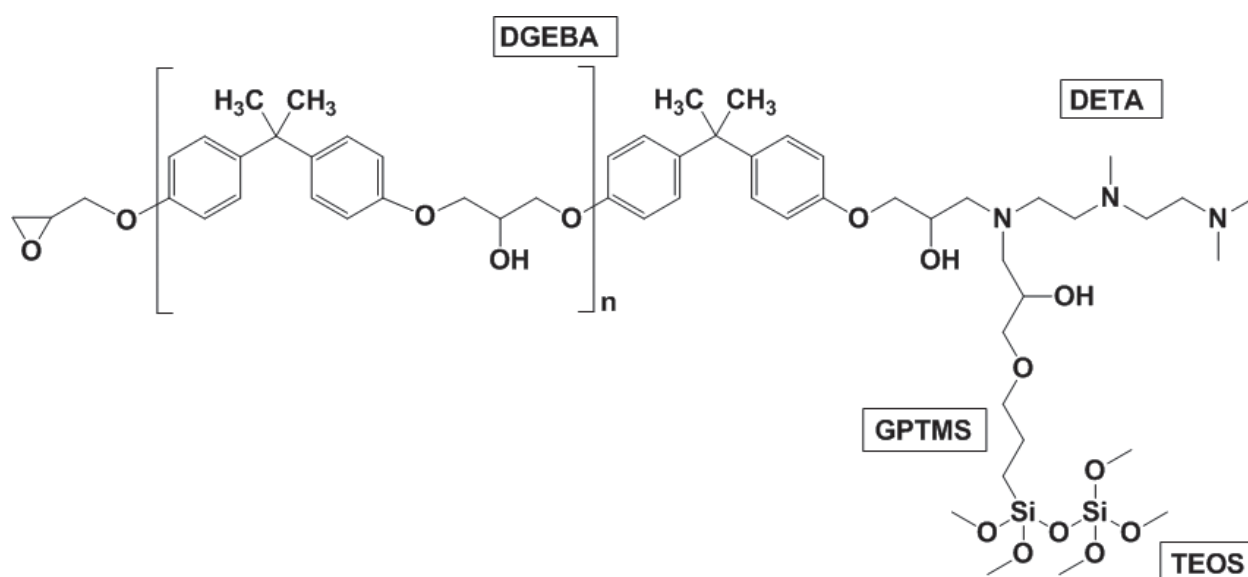

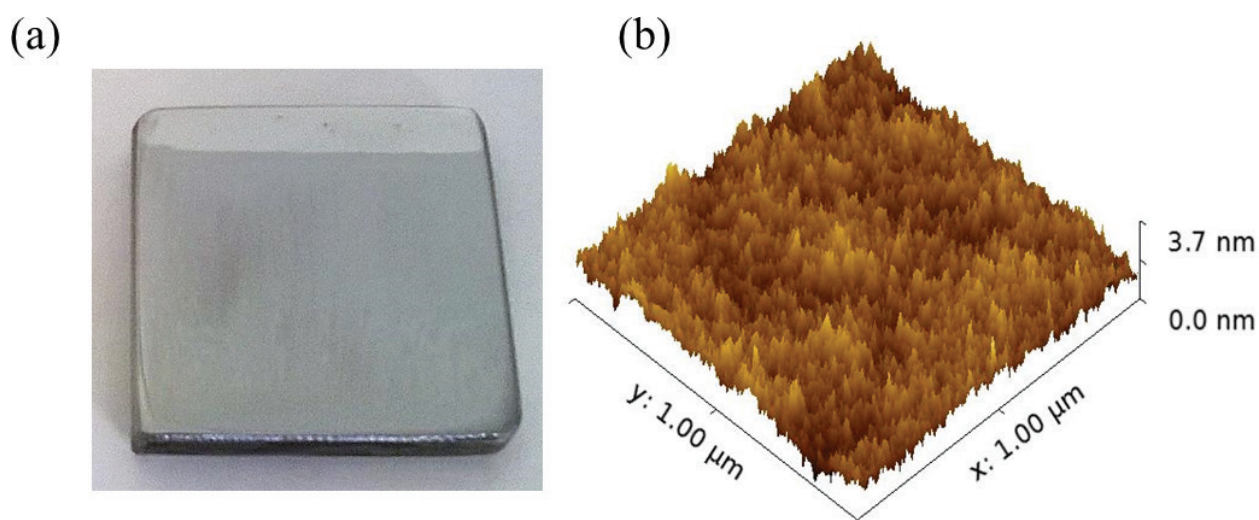**Figure 8.** Molecular structure of the epoxy-silica hybrid.

Figure 9. Representative image (a), and AFM image (b), of T1/G1 epoxy-silica hybrid coating deposited on carbon steel.

with an area of 1 μm² were used to obtain the surface roughness of the coatings. **Table 2** summarized all RMS surface roughness and thickness values determined for epoxy-silica hybrids of T-series (TEOS variation) and G-series (GPTMS variation). With increasing GPTMS and TEOS fraction, a significant increment of the surface roughness can be observed. The data suggest that increasing concentration of TEOS has a larger impact on the surface roughness than that of GPTMS, probably due to the formation of silica domains of larger size. Measurements of the films thickness indicate for all samples of the G-series a constant value of about 1.7 μm, while for films of the T-series the thickness varies from 2 to 3 μm, except for the T1.5 sample having 6.7 μm.

Samples	Thickness (μm)	RMS roughness (nm)	C_d (%)	α	R_g (nm)	d (nm)	T_0 (°C)	EIS lifetime (days)
T0	3.0	0.3	–	–	–	3.7	–	–
T0.5	2.0	0.7	85.0	3.8	–	4.2	306	2
T1/G1	1.6	1.2	83.8	3.2	0.8	–	293	5
T1.5	6.7	0.3	87.1	3.9	0.8	–	314	42
T2	3.3	2.6	87.8	3.5	0.8	–	295	1
T2.5	1.8	5	–	3.4	0.8	–	302	4
G0.0	1.0	–	–	3.8	–	–	–	–
G0.5	1.8	0.6	87.8	1.8	1.5	–	285	55
G1.5	1.8	0.4	94.7	4.0	0.6	–	297	–
G2	1.6	1.0	–	4.0	0.4	–	304	1
G2.5	1.8	1.4	–	4.0	0.3	–	306	2

Table 2. Properties of epoxy-silica hybrids: film thickness (optical interferometry); surface roughness (AFM); degree of polycondensation, C_d, (²⁹Si-NMR); Porod coefficient, α, radius of gyration, R_g, and correlation distance, d, (SAXS); temperature of the limit of thermal stability T_0 in N_2 atmosphere (TGA); and coating lifetime in 3.5% NaCl (EIS).

	G0.5		G2.5		T0.5		T2.5	
	XPS	Nominal	XPS	Nominal (at.%)*	XPS	Nominal	XPS	Nominal
Si 2p	4.8	4.3	6.3	6.0	4.4	4.0	7.5	7.6
C 1s	67.7	71.0	62.7	66.0	70.1	71	62.1	61.8
O 1s	25.5	22.0	28.1	25.0	22.9	22.3	28.1	28.1
N 1s	2.0	2.5	2.8	3.5	2.5	3	2.4	2.6
C/Si	14.1	16.9	10.0	11.0	15.9	19	8.3	8.1

*XPS experimental error ±5%.

Table 3. Comparison between XPS and calculated nominal atomic concentrations for epoxy-silica coatings.

Table 3 shows that results of the quantitative XPS analysis are in good agreement with those obtained for the nominal composition for both series of samples. As expected, the data show an increase of silicon and oxygen atomic concentration for the G and T-series, while nitrogen content increases slightly only for the G-series due to the higher DETA content. As the structure of GPTMS contains also carbon atoms, its addition leads to a less pronounced increase of the Si content. As a consequence, for the G-series the decrease of the C/Si ratio from 14.1 (G0.5) to 10.0 (G2.5) was smaller than that observed for the T-series from 15.9 (T0.5) to 8.3 (T2.5).

The chemical bonding structure of the inorganic network can be characterized according to the proportion of different Si species having a fixed number of oxygen bridging silicon atoms bonded to one (central) silicon atom. A common notation is Q^j for orthosilicates ($0 \leq j \leq 4$), such as TEOS, and T^j for organically modified silicates ($0 \leq j \leq 3$), such as GPTMS, where j gives the number of Si–O–Si bridges attached to the silicon atom.

Figure 10 shows the ^{29}Si NMR spectra, fitted with Gaussian components, used to extract the proportion of Q^j and T^j species. It can be observed that the Q^4 and T^3 peaks (−107 ppm and −62 ppm, respectively) have the highest intensities in relation to the other components related to lower network connectivity. The degree of connectivity of the inorganic phase, the so-called degree of polycondensation, C_d, has been determined from the fitted ^{29}Si NMR spectra using the following equation:
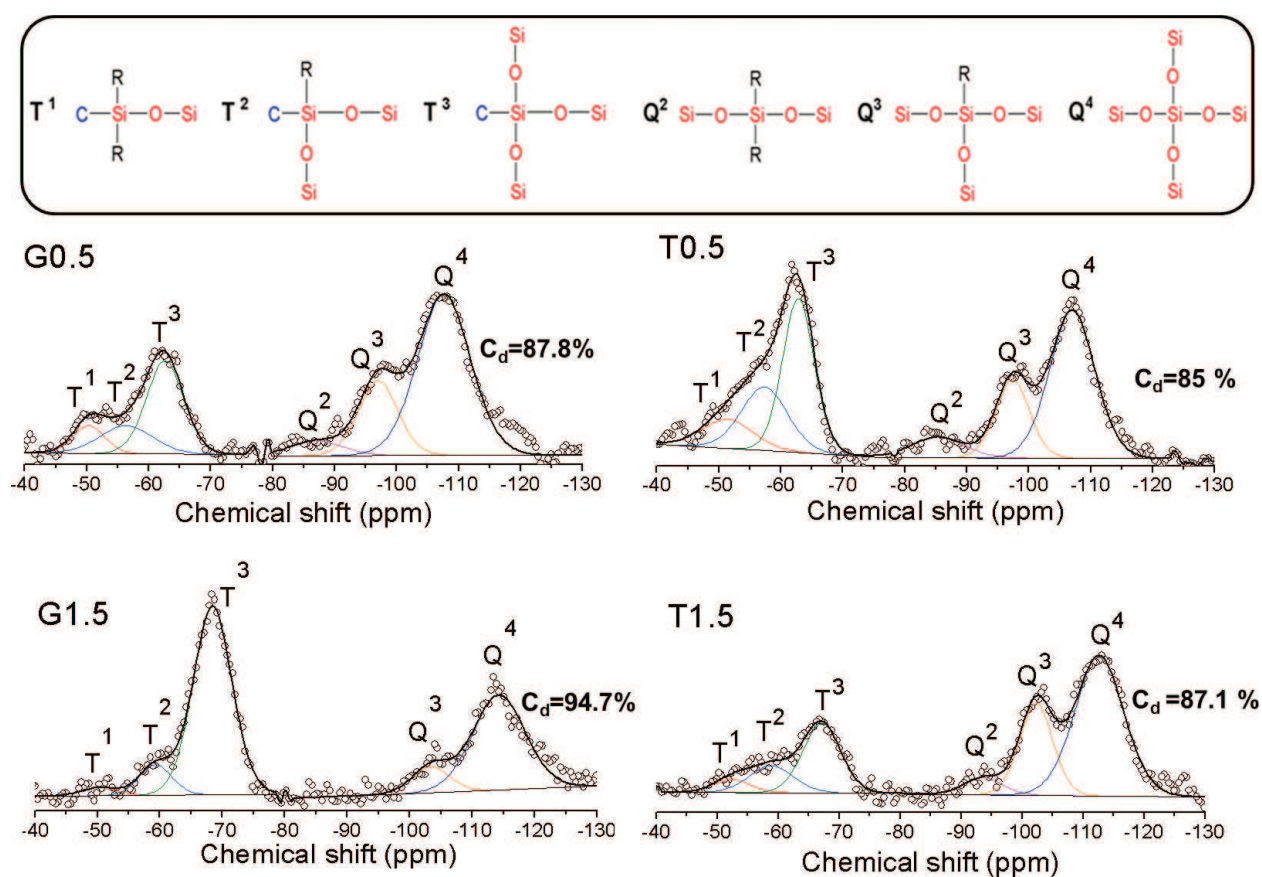

Figure 10. ^{29}Si-NMR spectra obtained for epoxy-silica hybrids. Inset: schematic representation of the T^j and Q^j species, where 'R' indicates OH or OCH_3 or OCH_2CH_3 groups.

$$C_d = \frac{T^1 + 2\,T^2 + 3\,T^3}{3} + \frac{Q^1 + 2\,Q^2 + 3\,Q^3 + 4\,Q^4}{4} \times 100 \qquad (4)$$

The C_d values of **Table 3** show a high connectivity of the inorganic network with a clear predominance of a tetra-substituted TEOS and a tri-substituted GPTMS sites. Furthermore, it seems that an increase of GPTMS favors the Q^4 and T^3 structures, yielding a highly cross-linked inorganic network reaching about 95% connectivity for G1.5 sample, while the variation of TEOS does not change the C_d values significantly, remaining in the range of 85–88%. More information on the structure and size of the inorganic domains was obtained by small angle X-ray scattering (SAXS) measurements.

The SAXS technique allows to access the nanostructural characteristics of the inorganic network due to the higher electronic density of silica compared that of the polymeric matrix. The log-log plots of scattering intensities I (q) recorded for different fractions of GPTMS and TEOS (**Figure 11**) show three main characteristics: a linear decay located at low q values, corresponding to the Porod region; a Gaussian decay in the mid q-range, corresponding to the Guinier regime; and a broad correlation peak superimposed to the Guinier region, observed only for T0.0 and T0.5 samples. The former feature, in the mid q-range, is characteristic of a diluted set scatters, while the latter is the result of the interferences of the scattered X-ray caused by the concentrated set of nano-objects.

These scattering patterns have been already observed for other silica-polymer hybrids [24, 25] and attributed to a hierarchical organization of silica nano-domains. Accordingly, we propose that the nanostructure of the hybrid can be described by a two-level hierarchical model, corresponding to a diluted or concentrated (T0.0 and T0.5) set of silica nanoparticles inside the aggregation zones embedded in the polymer matrix. In the case of the diluted system, the size of the smaller particles was determined, in terms of the radius of the gyration, R_g, by fitting the Gaussian decay observed in the mid q-range using the
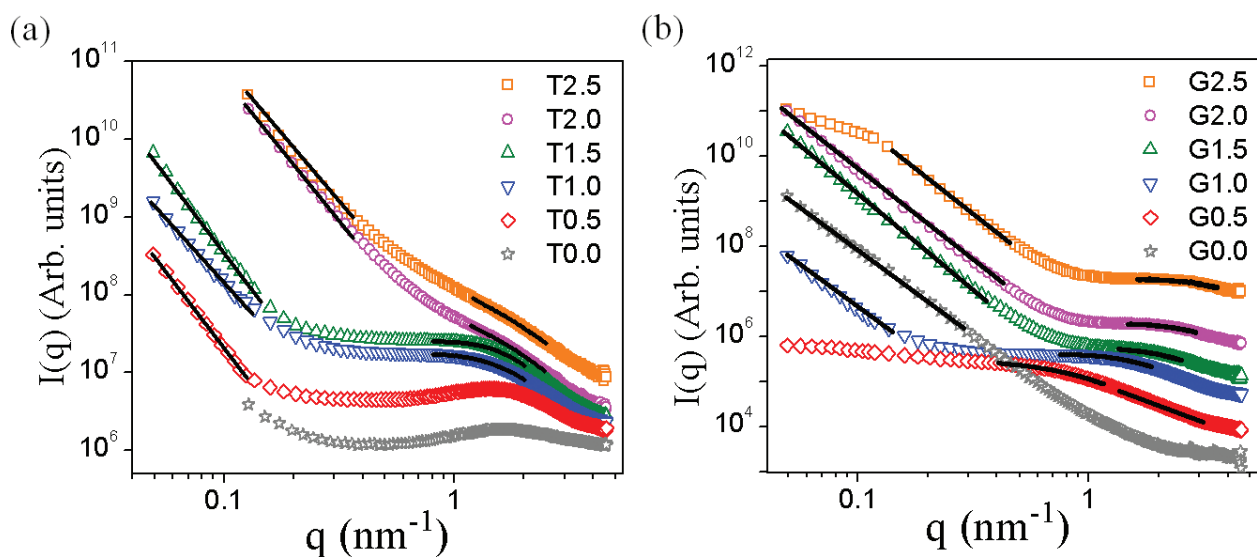

Figure 11. SAXS curves of T-series (a), and G-series (b), where the black lines represents the fits used to calculate the Porod coefficient (α) for q < 1 (except for the G0.5 sample, which presents α at q>1), and the radius of the gyration (R_g) for q >1. (The intensities were shifted to obtain a better visualization of the curves).

Guinier model: $I(q) = I_0 \exp(-R_g q^2/3)$, where I_0 is the scaling factor. However, this was only possible for scattering curves, which did not present an overlapping correlation peak. Therefore, values for R_g and those for the correlation distance, $d \approx 2\pi/q$, have been obtained only for a restricted number of samples (**Table 2**). Except for T0.0, the form of the scattering objects was determined by fitting the curves using the Porod model: $I \propto q^{-\alpha}$, where α is the Porod exponent. $\alpha \approx 4$ indicates a bi-phase system formed by set of nearly isometric scattering objects with a smooth surface, while for smaller values, a rough surface (fractal) is expected.

The results indicate that the inorganic phase consists of aggregates with relatively smooth surface and an average spacing of several nanometers ($d \approx 4$ nm). These domains have been formed by agglomeration of smaller silica particles with a size of about 1 nm ($0.3 < R_g < 1.5$ nm).

Some clear correlations between these parameters and the increasing silica concentration of the G- and T-series could be established. For the G-series, the evolution of the SAXS pattern evidences the role of GPTMS in controlling the size of primary silica particles and they aggregation. The power law decay over a decade and $\alpha = 3.8$ observed for the hybrid prepared only with TEOS (G0.0) characterizes the scattering by the surface of very large silica particles (>30 nm). The addition of a small amount of GPTMS (G0.5 sample) reduces the size of silica particles more than ten times ($R_g = 1.5$ nm) and prevents further aggregation, as evidenced by extended plateau at $q < 0.1$ nm. These unique features suggest for G0.5 sample an elevated nanostructural homogeneity, which might be responsible for the superior corrosion protection performance of this material (**Table 2**). In the case of the T-series, the correlation peak disappears for higher TEOS content and the linear decay shifts to higher q-values. These features evidence that TEOS addition favors the formation of more open aggregates, leading to a less compact nanostructure.

The thermal properties of the hybrids were studied by thermogravimetry under nitrogen flow. **Table 2** shows the temperature of the limit of thermal stability, T_0, for all epoxy-silica hybrids, defined as the temperature of 5% weight loss during the annealing process. The hybrids presented a thermal stability of about 300°C, relatively high values compared with those of other polymeric and hybrid materials [18, 22]. This advantageous property comes from the highly cross-linked structure provided by the curing agent (DETA) combined with the high polycondensation degree of the silica phase, as revealed by ^{29}Si NMR.

The anticorrosive performance of the hybrids was assessed by EIS measurements, in a 3.5% NaCl saline solution at 25°C. The hybrid coatings deposited on carbon steel were attached to an electrochemical cell, and after verifying a constant value of the open-circuit potential, the impedance measurements were performed as a function of time until a significative drop of the impedance modulus occurred. This time period was defined as lifetime of the coating, listed in **Table 2**. The impedance modulus at low frequency of the Bode plot is generally used as an indicator of the anticorrosive performance of the coating, with values higher than 0.1 GΩ cm^{-2} typically considered an excellent protection. The corrosion resistance of the films generally decreases with time, caused by the penetration of electrolyte into the protective layer through zones of residual porosity and defects.
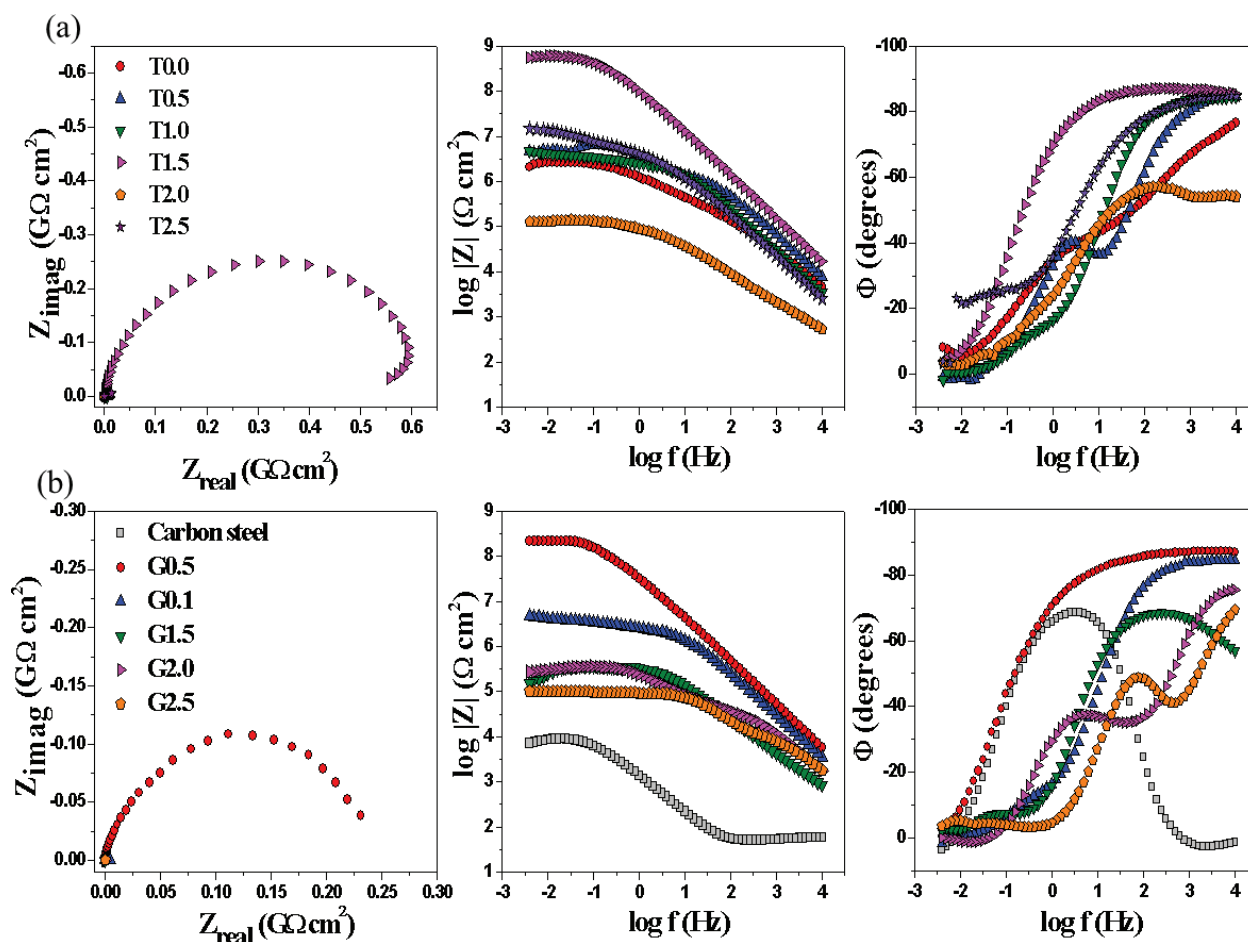
Figure 12. Nyquist and Bode plots of (a) series T and (b) series G of the epoxy-silica coatings deposited on carbon steel, compared to those of bare carbon steel, after 1 h of immersion in 3.5% NaCl solution.

The Nyquist and Bode plots obtained after 1 day of immersion in 3.5% NaCl solution are presented in **Figure 12**. It can be observed that two samples containing intermediate TEOS to GPTMS ratios (T1.5 and G0.5) presented the highest impedance modulus of 0.9 and 0.2 GΩ cm², respectively, and showed also the longest lifetime of several weeks (**Table 2**). These coatings show at higher frequencies (>1 Hz), a capacitive behavior with a phase angle higher than −80° extending over a range of 4 decades, characteristic for an efficient anticorrosive barrier layer. In contrast, for formulations with excess of TEOS or GPTMS, both the corrosion resistance and lifetime values show considerably lower values.

The results of the structural analysis indicate that the excellent barrier properties, found for coatings with intermediate TEOS to GPTMS ratio, result from a highly reticulated hybrid structure combining a number of favorable properties, such as a high polycondensation degree of the inorganic phase, a extremely smooth surface, indicating a very homogeneous distribution of silica nanodomains, high thermal stability, as well as an adequate quantity of the silica phase which ensures a good adhesion of the film to the metallic substrate. Although the corrosion protection efficiency of the best epoxy-silica coatings, reported so far [7, 26, 27], is comparable with results presented in this work, it may profit from their 10–100 times higher thickness.

3.2. PMMA-silica hybrids

Poly(methyl methacrylate), also known as acrylic and Pexiglas®, is a rigid, low cost, nontoxic, transparent and colorless thermoplastic polymer, extensively used as optical lenses, protective coatings, optical fibers, and as an alternative to glass in windows as well as a variety of household appliances. The introduction of an inorganic component, such as silica, improves the thermal stability, mechanical strength, and the adhesion to metallic substrates, the latter property being an essential feature for a high-efficiency coatings. The covalent bond between the PMMA and the silica phase can be achieved by the addition of 3-(trimethoxysilyl)propyl methacrylate (MPTS), a coupling agent formed by an alkoxy-silane group attached by a non-hydrolysable Si–C bond to the acrylic tail, which polymerizes with PMMA chains, while the inorganic part reacts with the silica precursor (TEOS), yielding an organic-inorganic hybrid structure, shown in **Figure 13**.

A variety of PMMA-silica hybrids have been studied, changing the organic/inorganic phase proportion, the amount of thermal initiator, the synthesis temperature and time, as well as the ethanol-to-water ratio. Furthermore, cerium salt has been added to the PMMA-silica matrix as corrosion inhibitor, and lignin, carbon nanotubes, and graphene oxide as fillers. The main results, found for pure PMMA-silica hybrids, are summarized in **Table 4**, those obtained using additives will be discussed in the following sections.

Similar to epoxy-silica coatings, PMMA-silica hybrids deposited on metallic substrates were homogeneous, transparent and had a very smooth surface. Structural analysis of PMMA-silica hybrids, performed by AFM, SAXS, NMR and XPS, has shown that the nanostructure is formed by a dense amorphous network of ramified silica-siloxane cross-link nodes, covalently interconnected by short PMMA chain segments [10, 22]. Varying the MMA/MPTS molar ratio from 2 to 10, NMR and SAXS results have shown that the M8 sample (MMA/MPTS = 8) presented the highest degree of polycondensation (83.9%) of the silica nanoparticles with an average radius of 0.8 nm, spaced by PMMA segments over an average distance of 4.6 nm. This coating exhibited also an excellent adhesion to the substrate (detachment force > 3.5 MPa) and the best anti-corrosion performance [10, 22]. EIS and potentiodynamic polarization results have shown that the M8 coating deposited on carbon steel acts as a very efficient corrosion barrier, increasing the total corrosion resistance by almost 6 orders of magnitude (>1 GΩ cm²) and reducing the current densities by more than 4 orders of magnitude (<0.1 nA cm⁻²), compared to the bare steel substrate [22]. Furthermore, XPS analysis confirmed that no corrosion-induced changes had occurred after 18 days of immersion in 3.5% NaCl solution [22].

Increasing the synthesis temperature from 70 to 80°C and the time of reaction from 2 to 4 h (sample M8_4h), an increase in the amount of polymeric phase was detected yielding a more compact and durable coating (56 days) [18, 22]. After optimizing also the ethanol-to-water ratio of the inorganic phase to a value of 0.2, the corrosion resistance and lifetime were further increase to 196 days in 3.5% NaCl (M8_4h_E0.2 coating, **Table 4**) [10]. Other important finding was the improvement of the corrosion resistance by hot deposition (M8_T80B0.01), which enhances the reaction between the inorganic phase and the metal substrate, improving the coating adhesion. This sample has been also deposited on Al2024 substrate and tested in saline (**Figure 14a**) and saline/acid environment (**Figure 14b**). This coating highlights a
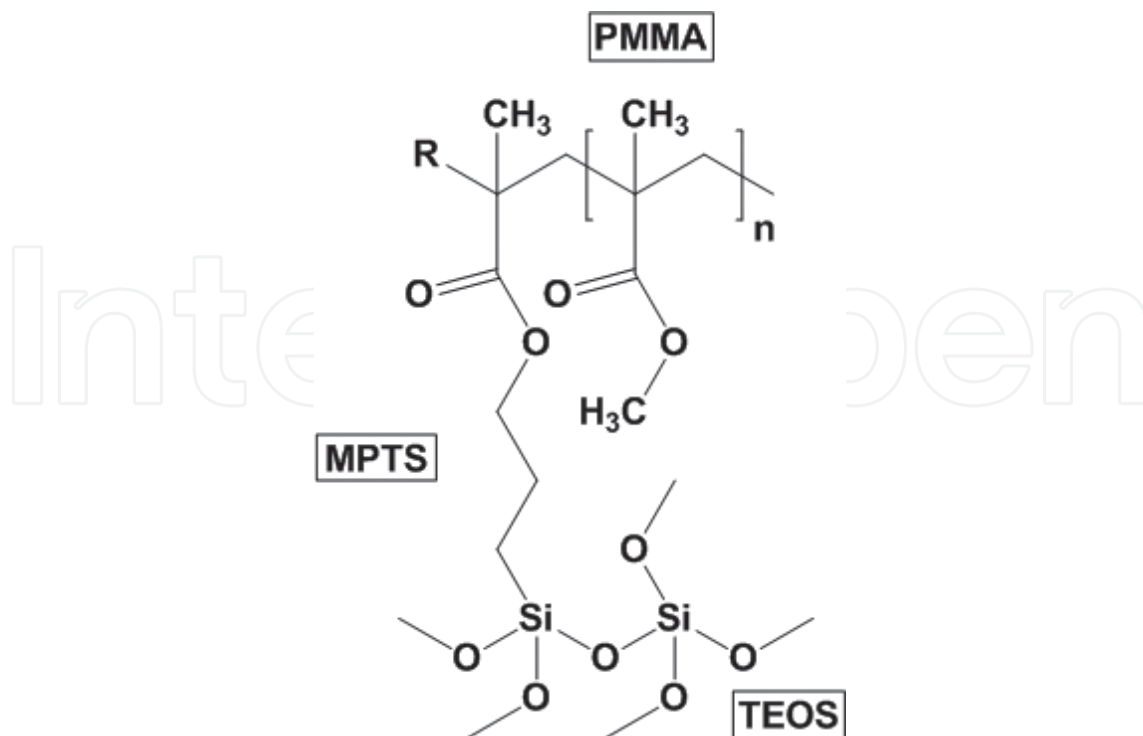
Figure 13. Molecular structure of the PMMA-silica hybrid.

Samples	Thickness (μm)	RMS roughness (nm)	C_d (%)	T_0 (°C)	$|Z|$ (GΩ cm²)	EIS lifetime (days)	Reference
M2	1.5	–	80.9	–	~0.001	–	[21]
M4	–	–	79.7	–	~0.01	–	[21]
M8	3	0.3	83.9	–	~1	18	[21]
M10	–	–	75.8	–	~0.001	–	[21]
M8_4h	2.8	0.4	78.0	205	~0.1	56	[18]
M8_4h_E0.2	2.0	0.5	82.0	230	~3	196	[10]
M8_T80B0.01	2.8	–	–	230	~3	40	–
M8_T80B0.01*	3.0	–	–	–	~50	560	–
M8_T90	2.6	–	–	238	~5	34	–
M8_T100	2.5	–	–	250	~0.1	35	–
M8_B0.05	5.0	–	–	270	~10	42	–
M8_B0.10	9.7	–	–	223	~10	>186	–

*Al2024 substrate.

Table 4. Properties of PMMA-silica hybrid coatings: film thickness (optical interferometry); surface roughness (AFM); degree of polycondensation, C_d, (²⁹Si-NMR); limit of thermal stability T_0 in N_2 atmosphere (TGA); impedance modulus $|Z|$, after 1 day exposure to 3.5% NaCl solution (EIS); and coating lifetime in 3.5% NaCl (EIS).

corrosion resistance of up to 50 GΩ cm², in saline environment, showing only a small performance decrease to 0.1 GΩ cm² after 560 days exposure. This is to our best knowledge the highest durability, obtained so far for hybrid coatings in standard saline solution. Also in contact with a saline/acid solution (0.05 mol L⁻¹ H₂SO₄ + 0.05 mol L⁻¹ NaCl), this about 3-μm thick coating presented a high corrosion resistance (20 GΩ cm²), remaining almost unchanged during its lifetime of 87 days. It is interesting to note that the phase angle dependence has a capacitive behavior (θ ≈ −90°), over a frequency range of 6 decades, a behavior close to that of an ideal capacitor, highlighting the extraordinary performance of this coating.

PMMA-silica hybrids have been also prepared at different synthesis temperatures of the organic precursor (80–100°C) and different BPO/MMA molar ratio (0.01–0.1), using the well-established MMA/MPTS molar ratio of 8 [22]. The increase in the synthesis temperature did not influence significantly the structure, the thermal properties and the corrosion resistance, however, the increase of the BPO amount led to an increase of the polymerization degree, thermal stability of 40°C (BPO0.05), and also of the anticorrosive efficiency (**Table 4**). The sample M8_BPO0.05 and M8_BPO0.10 presented an impedance modulus of 10 GΩ cm² in a saline medium (3.5% NaCl), remaining essentially unchanged during more than 6 months of exposure (M8_BPO0.10).
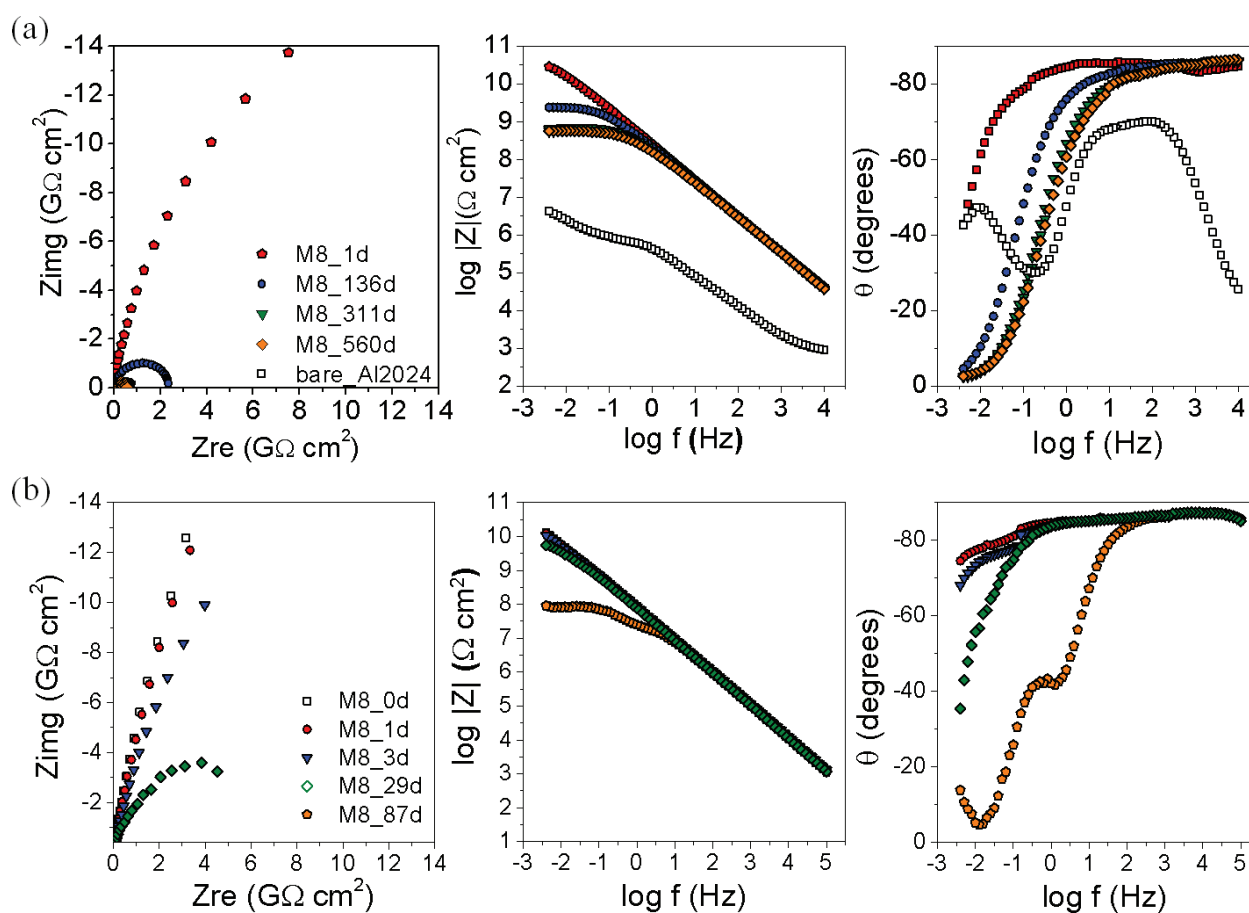

Figure 14. Time dependence of Nyquist and Bode plots of the M8_T80BPO0.01 PMMA-silica coating deposited on Al2024 substrate in contact with a) in 3.5% NaCl solution and b) 0.05 mol L⁻¹ NaCl + 0.05 mol L⁻¹ H₂SO₄ solution.

3.3. PMMA-silica hybrid modified with Ce(IV) salt for self-healing ability

After identifying the optimum proportion of polymeric and silica phase for the formation of a highly ramified structure (MMA/MPTS/TEOS molar ratio = 8/1/2), increasing molar percentage of Ce(IV) ions (0.1% < Ce/Si < 5%) have been added to the inorganic precursor to enhance the passivating character of the films [11].

NMR, XPS, and SAXS results, summarized in **Table 5**, have revealed the active role of Ce(IV) in the PMMA-silica matrix. The correlation of XPS and NMR data evidenced that the Ce(IV) concentration is directly related to the polycondensation degree (C_d) and the degree of Ce(IV) reduction, both decreasing with increasing cerium concentration. Low concentrations of cerium lead to an enhanced polycondensation of the siloxane/silica phase, with connectivity of the inorganic phase up to 87%. For low doping levels of Ce/Si < 0.7%, SAXS results have revealed increasing values of radius of gyration, R_g, suggesting an active role of Ce(IV) as oxidation agent in the enhanced growth of a cross-linked and polycondensed inorganic phase. Detailed investigation of the structural effects of cerium species has shown that reduction of Ce(IV) ions not only catalyzes a higher connectivity of the silica phase, but also enhances the polymerization of organic moieties. The resulting enhancement of the overall network connectivity leads to an improvement of the thermal stability of the hybrids, as evidenced by the results of the thermogravimetric analysis [11].

The electrochemical assays, performed by EIS and potentiodynamic polarization curves, have shown that the PMMA-silica coatings containing intermediate concentrations of cerium present a combination of high-corrosion resistance (~10 GΩ cm^2), elevated overpotential stability at low-current densities (<10^{-11} A), as well as excellent long-term stability of up to 304 days. Compared to the bare carbon steel substrate, the coated samples showed up to 6 orders of magnitude higher impedance modulus and up to 6 orders of magnitude lower current densities [11].

For coatings containing elevated Ce(IV) doping levels (Si/Ce = 5%), the self-healing effect was observed, induced by the formation of insoluble cerium oxides and hydroxides in corrosion affected regions. The presence of these phases in the near surface region was evidenced by XPS O 1s spectra and by scanning electron microscopy, showing the presence of nanopits (<300 nm). It was suggested that these phases were formed by reactions of Ce(III) and Ce(IV) with water and residual hydroxyl groups of the hybrid. The self-healing process prevented the progression of the corrosion process for more than 13 months keeping the corrosion resistance constant above 0.01 GΩ cm^2. The excellent anticorrosive efficiency achieved by PMMA-silica coatings containing cerium can be related to a double effect of Ce(IV), combining the densification of the hybrid network with the formation of insoluble cerium species in regions affected by pitting [11].

3.4. PMMA-silica hybrid reinforced with lignin, carbon nanotubes and graphene oxide

Lignin is a macromolecule present in the cell walls of terrestrial plants that confers rigidity and impermeability, usually corresponding to 15–30% of the dry weight of wood (**Figure 15a**).

Properties	Ce(IV)/Si molar fraction (%)								
	0	0.1	0.2	0.3	0.5	0.7	1	3	5
C_d (%)	82.8	87.1	–	83.6	82.7	79.3	78.5	77.6	77.3
XPS Ce(IV) fraction (%)	–	–	–	28.5 ± 4	37.2 ± 3	46.4 ± 2.5	48.5 ± 2.5	55.5 ± 2	60.4 ± 1.5
R_g (nm)	0.9	1.1	1.8	2.3	2.3	1.9	1.9	–	–
$|Z|$ (GΩ cm^2)	~0.5	~0.5	–	–	~0.1	~10	~5	–	~0.5
Lifetime (days)	42	85	–	96	–	304	65	48	404

Table 5. Properties of PMMA-silica hybrids containing different amounts of Ce(IV): degree of polycondensation, C_d, (^{29}Si-NMR); percentage of the Ce(IV) oxidation state (XPS Ce 3d spectra); radius of gyration, R_g, (SAXS); and impedance modulus, $|Z|$, after 1 day exposure to 3.5% NaCl solution (EIS).

Presently, millions of tons of lignin are generated from biodiesel and ethanol production, and most part is incinerated to generate electric energy. However, nobler applications have been found to add value to this biomass, such as the reinforcement of different classes of materials. Properties, such as low density, low abrasive character, hydrophobicity, and low cost, make lignin ideal to use as filler in polymeric and organic-inorganic hybrid matrices [20].

Carbon nanotubes (CNTs) and graphene oxide (GO) (**Figure 15b and c**) are also very interesting nanofillers for the structural reinforcement of polymeric and hybrid materials, due to their exceptional thermal, chemical, and mechanical resistance. Both present a hexagonal sp^2 arrangement of carbon atoms, forming extremely stable cylindrical and monolayer structures, respectively. Graphene oxide has been obtained from oxidation and exfoliation of graphite, yielding a graphene layer containing oxygen functional groups such as epoxy, hydroxyl, and carboxyl [18].

PMMA-silica hybrids reinforced with 0.05, 0.10, 0.50 and 1.00 wt.% of lignin have been deposited on carbon steel by dip-coating, producing about 2.5 μm thick coatings (**Table 6**). Optical microscopy and optical microscopy and atomic force microscopy showed that lignin was well dispersed in the hybrid matrix, and all coatings presented a low RMS surface roughness between 0.3 and 0.4 nm. The introduction of lignin in the PMMA-silica hybrid increased the water contact angle of the film surface from 79.3° to 87.9°, the hardness from 22.9 to 30.9 HV, and the scratch resistance (critical load for delamination) from 55 to 80 mN. In addition, the thermal degradation events, obtained by thermogravimetric analysis (TGA) under nitrogen atmosphere, were shifted to higher temperatures with lignin addition, due to its phenolic structure which has the ability to trap radicals formed during the depolymerisation. Besides increasing the thermal stability of the polymeric phase, it acts also as UV stabilizer [20].

The electrochemical tests performed by EIS showed that the PMMA-silica coatings containing lignin act as efficient diffusion barriers, with corrosion resistance higher than 0.1 GΩ cm^2 after
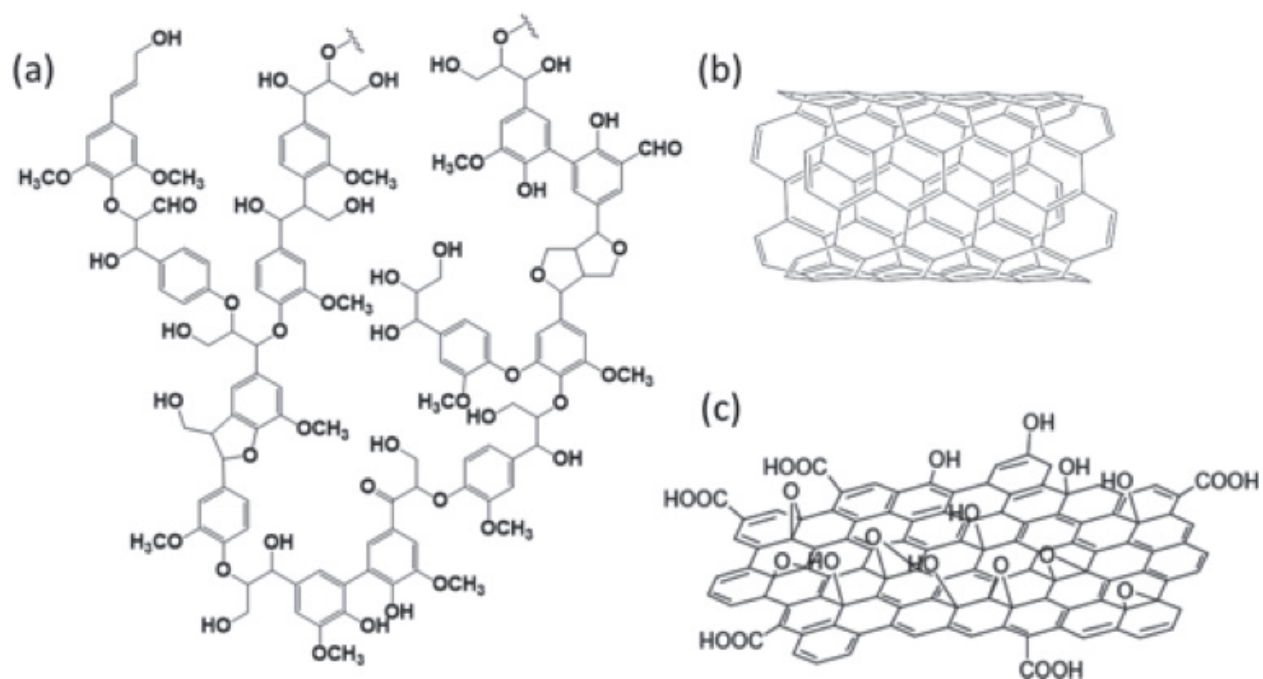
Figure 15. Molecular structure of (a) lignin, (b) carbon nanotube, and (c) graphene oxide.

Sample	Thickness (μm)	T_0 (°C)	Critical load (mN)	|Z| (GΩ cm²)	EIS lifetime (days)	Reference
M8 (70°C/2 h)	2.4	170	55	~0.1	18	[20]
M8_lignin_0.50 wt.%	2.6	180	65	~0.5	–	[20]
M8_lignin_0.10 wt.%	2.5	200	80	~0.5	50	[20]
M8_lignin_0.50 wt.%	2.7	190	66	~0.01	–	[20]
M8_lignin_1.00 wt.%	2.7	195	56	~0.005	–	[20]
M8_BPO001 (80°C/4 h)	2.8	205	78	~0.5	56	[18]
M8_BPO001_ CNT_0.05%	5.7	220	–	~0.1	43	[18]
M8_BPO001_ GO_0.05%	3.1	275	94	~1	203	[18]
M8_BPO005 (80°C/4 h)	3.5	208	84	~1	21	[18]
M8_BPO005_ CNT_0.05%	6.6	209	133	~10	7	[18]
M8_BPO005_ GO_0.05%	5.5	216	148	~5	168	[18]

Table 6. Properties of PMMA-silica hybrids containing lignin, CNT or GO: film thickness (optical interferometry); limit of thermal stability T_0 in N_2 atmosphere (TGA); critical load for delamination (microscrach test); impedance modulus \|Z\|, after 1 day exposure to 3.5% NaCl solution (EIS); and coating lifetime in 3.5% NaCl (EIS).

exposure to 3.5% NaCl aqueous solution. For intermediate lignin content of 0.10 wt.% the coatings presented best results with an impedance modulus of 0.5 GΩ cm^2, remaining almost unchanged after 50 days of exposure to aggressive environment [20].

Recent studies on the inclusion of carbon nanotubes and graphene oxide in hybrid and polymer matrices have shown excellent results in terms of increased mechanical strength, scratch and wear resistance, thermal stability, adhesion to metallic substrate, hydrophobicity, and electrical conductivity [18, 19, 28–30]. Despite all of these advances, a simultaneous improvement not only of mechanical and thermal stability but also of anticorrosive efficiency of protective coatings has been accomplished only recently by the incorporation CNT and GO in a PMMA-silica matrix [18].

To synthesize the CNT and GO modified PMMA-silica hybrids, first, the single-walled carbon nanotubes and graphene oxide were dispersed in a water/ethanol, adding in the case of CNTs dodecyl sulfate surfactant (SDS) as dispersant. Then, the carbon nanostructures were added to the inorganic precursor solution of the PMMA-silica hybrid at a carbon (CNT or GO) to silicon (TEOS and MPTS) molar ratio of 0.05% in two different matrices, prepared at BPO/MMA molar ratios of 0.01 and 0.05. As the function of BPO as a thermal initiator is to produce radicals that initiate the polymerization process of MMA, an increased BPO content results in enhanced polymerization degree in the hybrid. The transparent hybrids deposited on A1020 carbon steel substrates by dip coating presented thickness values between 2.8 and 6.6 μm (**Table 6**), a good dispersion of the carbon nanostructures, and a very smooth surface (0.3–0.5 nm RMS surface roughness) [18].

Microscratch and wear tests, performed with a spherical-conical diamond tip of 10 μm radius, confirmed for the PMMA-silica coatings that both additives, CNT and GO, improved the scratch resistance (increase of the friction coefficient by 0.1–0.2), adhesion to the metallic substrate (no delamination for M8_BPO001_CNT up to 240 mN) and wear resistance (smooth and shallow wear track after 50 cycles). The superior behavior of CNT containing coatings was attributed to their property to act as rigid obstacles for the scratch tip. Results of the thermogravimetric analysis have shown that the addition of CNT and GO to the BPO0.01 matrix and to a smaller extent to the BPO0.05 matrix, increased the thermal stability of the hybrids up to 70°C for GO containing samples (**Table 6**). This improvement was attributed to interaction between carbon nanostructures and macroradicals generated during the process of depolymerisation combined with a 2D barrier effect of GO, hindering molecular diffusion through the matrix and thus providing an improved thermal resistance [18].

Results of electrochemical impedance spectroscopy in 3.5% NaCl solution showed that PMMA-silica coatings reinforced with CNTs and GO had an improved anticorrosive efficiency, with impedance modulus of ~1 GΩ cm^2 and ~10 GΩ cm^2 for the BPO0.01 and BPO0.05 matrix, respectively. Besides the improved barrier property, GO containing coatings presented also a prolonged lifetime of up to 203 days. This was attributed to the two dimensionality of the GO structure that provides an enhanced barrier effect against the propagation of corrosive species. Furthermore, it was suggested that both carbon nanostructures act as densifiers of

the nanocomposite and also as negatively charged repulsive agents for chloride anions, thus improving barrier property of the coating. Based on the equivalent circuit used to fit the EIS data, this notable barrier behavior was interpreted, in terms of two distinct dielectric layers, one related to a porous water uptake zone at the coating/electrolyte interface and the other corresponding to the underlying unaffected film region, having three orders of magnitude higher resistivity [18].

3.5. Advances in organic-inorganic hybrid coatings for corrosion protection

To be able to evaluate the relevance of the obtained results, it is important to place them in the context of the state of the art in the field of anticorrosive coatings. In the last decade, the concept of organic-inorganic hybrids as protective coating has been intensely investigated using different approaches involving a variety of organic and inorganic precursor reagents, resulting in a number of promising coatings systems. The most widely applied formulations for hybrid phases used to prepare high-performance anticorrosive coatings are based on epoxy-silica (**Table 7**) and acrylic-silica (**Table 8**) hybrids, and to a lower extent on polyurethane-silica, polyurethane-silica-zirconia and other epoxy systems (**Table 9**). As can be inferred from these data, the electrochemical barrier properties, obtained for different hybrid formulations, have achieved a notable performance in the last years, making these novel nanocomposites very promising candidates for efficient corrosion protection of metallic surfaces. This is justified especially when considering that a high-corrosion resistance and long durability in aggressive environments can be achieved by thin films with thicknesses of less than 10 μm, resulting in substantially reduced material costs compared to conventional high-performance coating systems. More specifically, regarding the epoxy-silica hybrid system, the results presented in this work and those listed in **Table 7** show that different compositions applied to distinct alloys can provide a very effective long-term corrosion protection [7, 26, 27]. Very promising results were also achieved for PMMA-silica coatings [8, 10, 31], with the highest observed durability of more than 560 days in 3.5% NaCl, and for hybrids containing reinforcement and inhibitor agents [11, 18]. Moreover, for some polyurethane-silica and polyurethane-zirconia-silica systems, it has been demonstrated that they also have a high potential to be used as efficient anticorrosive barrier layers [9, 32].

All these results demonstrate the wealth of possibilities to prepare nanocomposite materials based on organic-inorganic hybrids in the form of highly efficient anticorrosive coatings. The optimization of the barrier property can be achieved by the careful adjustment of the precursor proportions, including coupling agents and additives, together with the conditions of synthesis, deposition, and thermal treatment. However, the main key for this task is an in-depth knowledge of the formation mechanisms as well as the compositional and structural properties of the material. Based on this information, it was shown that a relatively simple preparation process yields highly efficient and very durable anticorrosive films. They unite three essential perquisites for an appropriate coating system: a high corrosion resistance, long-term stability, and environmental compatibility. Considering also the simplicity

of the sol-gel process and the low material consumption, which scales with the film thickness, these about 5-μm thick hybrid films constitute from the economical and environmental point of view a very interesting alternative for conventional protective coating systems.

Hybrid	Synthesis	Substrate	Deposition/ thickness (μm)	EIS: |Z| (GΩ cm²), lifetime (days), solution	Polarization I_{corr} (A cm⁻²) E_{corr} (V), reference electrode	Reference
Epoxy-GPTMS-TEOS	Sol-gel	Carbon steel	Dip-coating/6.7	~1 42 3.5% NaCl	_ −0.08 Ag/AgCl	[This work]
Epoxy-APTES-ZnO	Sol-gel	Mg alloy AZ31	Dip-coating/~12	~1 35 0.05 M NaCl	_	[33]
Epoxy-APTES	_	Carbon steel	Spray/125	~100 21 0.1 M Na₂SO₄	_	[27]
Epoxy-SiO₂	Sol-gel	Mg alloy	Dip-coating/-	~100 7 3.5% NaCl	_	[34]
Epoxy-APTES	Solution intercalation method	Mild steel	Brush method/70–80	~10 30 3% NaCl	_	[35]
Epoxy-APTES-tetrathiol	Sol-gel	Al alloy AA2024-T3	Single blade/150	~1 350 0.5 M NaCl	_	[26]
Epoxy-polysiloxane	Commercial	Cold rolled low carbon steel	Air-less spray/70	~100 467 3% NaCl	_ −0.65 SCE	[7]
GPTMS-MTEOS-TEOS	Sol-gel	Al alloy AA2024-T3	Dip-coating/25	~0.1 38 5% NaCl	_	[36]
Epoxy-APTES	_	Mg alloy AZ31	Dip-coating/14	~10 31 0.5 M NaCl	_	[37]
Epoxy-GPTMS-MTEOS/-	Sol-gel	Al alloy AA2024	Dip-coating/~8	~1 51 0.05 M NaCl	10^{-10} −0.3 Ag/AgCl	[38]

GPTMS: (3-glycidoxypropyl)trimethoxysilane; TEOS: tetraethoxysilane; APTES: aminopropyl-triethoxysilane; tetrathiol: pentaerythritol tetrakis(3-mercaptopropionate); MTEOS: methyl-triethoxysilane; SCE: standard calomel electrode.

Table 7. Principal preparation parameters and results reported for epoxy-silica coatings applied for corrosion protection of metallic surfaces, including corrosion resistance |Z|, current density, I_{corr}, and corrosion potential, E_{corr}.

Hybrid/additive	Synthesis	Substrate	Deposition/ thickness (µm)	EIS: |Z| (GΩ cm²), lifetime (days), solution	Polarization I_{corr} (A cm^{-2}) E_{corr} (V), reference electrode	Reference
PMMA-MPTS-TEOS/-	Radical polymerization and sol-gel	Al alloy AA2024	Dip-coating/~3	~50 more than 560 3.5% NaCl	– −0.68 Ag/AgCl	[This work]
PMMA-MPTS-TEOS/-	Sol-gel	316L stainless steel	Dip-coating/~2	~0.01 36 3.5% NaCl	10^{-9} 0.1 Ag/AgCl	[14]
GMA-EHA-GPTMS-TEOS/-	Sol-gel	Al alloys AA1050	Spin-coating/~1	~1 21 0.1 M NaCl	–	[39]
PMMA-MPTS-TEOS/-	Sol-gel	A1010 carbon steel	Dip-coating/1.5–3	~1 18 3.5% NaCl	10^{-10} −0.3 Ag/AgCl	[22]
PMMA-MPTS-TEOS/ Ce(IV)	Radical polymerization and sol-gel	A1010 carbon steel	Dip-coating/~2	~10 304/404 3.5% NaCl	10^{-11} + 0.3 Ag/AgCl	[11]
PMMA-MPTS-TEOS/ lignin	Radical polymerization and sol-gel	A1020 carbon steel	Dip-coating/~2	~0.5 50 3.5% NaCl	–	[20]
PMMA-MPTS-TEOS/-	Radical polymerization and sol-gel	A1010 carbon steel	Dip-coating/1.5–2	~5 196 3.5% NaCl	–	[10]
PMMA-MPTSTEOS/ Ce	Sol-gel	Mild steel	Dip-coating/~26	~10 362 3.5% NaCl	10^{-12} + 0.35 SCE	[31]
Acrylic resin-SiO$_2$/-	Solution intercalation method	Mild steel	Brush method/75	~10 90 3.5% NaCl	–	[8]
Acrylic resin-silanol-ZnO/-	Solution intercalation method	Mild steel	Brush method/75	~10 30 3.5% NaCl	–	[40]
PMMA-MPTS-TEOS/CNTs, GO	Radical polymerization and sol-gel	A1020 carbon steel	Dip-coating/3–6	~3 211 3.5% NaCl	– +0.58 Ag/AgCl	[18]

PMMA: poly(methyl methacrylate); MPTS: 3-(trimethoxysilyl)propyl methacrylate; TEOS: tetraethoxysilane; GMA: glycidyl methacrylate; EHA: 2-ethylhexyl acrylate; GPTMS: (3-glycidoxypropyl) trimethoxysilane;CNTs: carbon nanotubes; GO:graphene oxide; SCE: standard calomel electrode.

Table 8. Principal preparation parameters and results reported for acrylic-silica coatings applied for corrosion protection of metallic surfaces, including corrosion resistance \|Z\|, current density I_{corr}, and corrosion potential E_{corr}.

Hybrid/additive	Synthesis	Substrate	Deposition/ thickness (μm)	EIS: |Z| (GΩ cm²), lifetime (days), solution	Polarization, I_{corr} (A cm^{-2}), E_{corr} (V), reference electrode	Reference
Polyurethane APTES-TEOS/-	_	AA3003 H14	Drawdown bar/75	~100 263 3.5%NaCl+0.1M HCl	_	[9]
Polyurethane-ZrO$_2$-SiO$_2$/-	Sol-gel	Carbon steel	Spray/40–55	~100 226 3.5% NaCl	_	[32]
Epoxy-polyaniline-ZnO/-	Chemical oxidative method	Carbon steel	Dip-coating/118	~1 90 3.5% NaCl	_ −0.05 (SCE)	[41]
Polyetherimide-HA/-	_	Mg alloy AZ31	Dip-coating/~4	~1 101 Hank's solution	_	[42]
Epoxy-LDH/-	_	Al alloy AA2024-T3	Spray/55	~1 18 0.05M NaCl	_	[43]
Epoxy-HS/8-hydroyquinoline	_	Al alloy AA2024-T3	Dip-coating/~25	~1 90 0.5M NaCl	_	[44]
Epoxy-CaCO$_3$	_	Al alloy AA2024-T3	Dip-coating/~30	~1 41 0.5M NaCl	_	[45]
Epoxy-ester-siloxane-urea	_	Al alloy AA2024-T3	Drop-coating/130–140	~0.1 70 3.5% NaCl	10^{-10} −0.4 SCE	[46]

APTES: aminopropyltriethoxysilane; TEOS: tetraethoxysilane; HA: hydroxyapatite; LDH: Layered double hydroxide; HS: halloysites; CaCO$_3$: calcium carbonate; SCE: standard calomel electrode.

Table 9. Principal preparation parameters and results reported for a varied of hybrid coatings applied for corrosion protection of metallic surfaces, including corrosion resistance \|Z\|, current density I_{corr}, and corrosion potential E_{corr}.

4. Conclusions

Structural, thermal, mechanical, and electrochemical characterization of novel epoxy-silica and PMMA-silica hybrid coatings have shown that their properties are extremely dependent of the hybrid precursors proportion, time and temperature of synthesis, and addition of fillers. After a careful adjustment of the preparation conditions, these homogeneous and transparent hybrid coatings present a defect-free very smooth surface, low porosity, a highly cross-linked silica network, excellent adhesion to the metallic substrate, elevated thermal stability, and especially an excellent anticorrosive performance. Epoxy-silica and PMMA-silica films with thicknesses of less than 10 μm exhibit a dense and highly reticulated nanostructure, resulting in enhanced thermal stability combined with

high corrosion resistance and long durability in saline environment. Exceptional barrier properties, especially on aluminum alloy, were found for PMMA-silica hybrids prepared at a 8MMA:1MPTS:2TEOS molar ratio, 4 h/80°C of synthesis, and BPO/MMA molar ratio of 0.01. This coating highlights a corrosion resistance of about 50 GΩ cm^2 and a lifetime of more than 18 months in saline solution. Nanofillers have been successfully added to the PMMA-silica matrix to improve the anticorrosive performance and to reinforce the hybrid structure. Carbon nanotubes and graphene oxide incorporated into the PMMA-silica matrix resulted in a multifunctional material, which combines an excellent anticorrosive performance with improved adhesion, anti-scratch and heat-resistant properties, thus extending the application range of these coatings to abrasive environments. Furthermore, it has been shown that added Ce(IV) ions act as oxidation agents during the formation of the hybrid matrix, leading to densification process that improves the barrier property of the coatings. In addition, the active corrosion inhibition provided by formation of insoluble cerium species in regions affected by corrosion, known as self-healing ability, resulted in a prolonged the lifetime of the coatings. The great progress achieved in the last couple of years in the development of organic-inorganic hybrids makes these materials very promising candidates for new-generation high-performance protective coatings.

Acknowledgements

Author details

Samarah V. Harb, Andressa Trentin, Ruben F. O. Torrico, Sandra H. Pulcinelli, Celso V. Santilli and Peter Hammer*

*Address all correspondence to: peter@iq.unesp.br

Instituto de Química, UNESP-Universidade Estadual Paulista, Araraquara, SP, Brazil

References

[1]   Brasunas A. de S., Delinder L. S. V. Corrosion basics: An introduction. 1984. Houston: TX: National Association of Corrosion Engineers. 353 p.

[2]   Wint N., Vooys A. C. A., de McMurray H. N. The corrosion of chromium based coatings for packaging steel. Electrochimica Acta. 2016;**203**:326-336. DOI: 10.1016/j.electacta.2016.01.100.

[3]   Schem M., Schmidt T., Gerwann J., Wittmar M., Veith M., Thompson G. E., Molchan I. S., Hashimoto T., Skeldon P., Phani A. R., Santucci S., Zheludkevich M. L. CeO_2-filled sol-gel coatings for corrosion protection of AA2024-T3 aluminium alloy. Corrosion Science. 2009;**51**(10):2304-2315. DOI: 10.1016/j.corsci.2009.06.007.

[4]   Norouzi M., Garekani A. A. Corrosion protection by zirconia-based thin films deposited by a sol-gel spin coating method. Ceramics International. 2014;**40**(2):2857-2861. DOI: 10.1016/j.ceramint.2013.10.027.

[5]   Quinson J. F., Chino C., Becdelievre A. M. De, Guizard C., Brunel M. Deformation capability and protective role of zirconia coatings on stainless steel. Journal of Materials Science. 1996;**31**(19):5179-5184. DOI: 10.1007/BF00355922.

[6]   Sanchez C., Belleville P., Popall M., Nicole L. Applications of advanced hybrid organic-inorganic nanomaterials: From laboratory to market. Chemical Society Reviews. 2011;**40**(2):696-753. DOI: 10.1039/C0CS00136H.

[7]   Echeverría M., Abreu C. M., Lau K., Echeverría C. A. Viability of epoxy–siloxane hybrid coatings for preventing steel corrosion. Progress in Organic Coatings. 2016;**92**:29-43. DOI: 10.1016/j.porgcoat.2015.12.005.

[8]   Ammar S. H., Ramesh K., Vengadaesvaran B., Ramesh S., Arof A. K. A novel coating material that uses nano-sized SiO_2 particles to intensify hydrophobicity and corrosion protection properties. Electrochimica Acta. 2016;**220**:417-426. DOI: 10.1016/j.electacta.2016.10.099.

[9]   Visuet E. M., Gao T., Soucek M., Castaneda H. The effect of TiO_2 as a pigment in a polyurethane/polysiloxane hybrid coating/aluminum interface based on damage evolution. Progress in Organic Coatings. 2015;**83**:36-46. DOI: 10.1016/j.porgcoat.2015.02.001.

[10] dos Santos F. C., Harb S. V., Menu M., Turq V., Pulcinelli S. H., Santilli C. V., Hammer P. On the structure of high performance anticorrosive PMMA-siloxane-silica hybrid coatings. RSC Advances. 2015;**5**(129):106754-106763. DOI: 10.1039/c5ra20885h.

[11] Harb S. V., dos Santos F. C., Caetano B. L., Pulcinelli S. H., Santilli C. V., Hammer P. Structural properties of cerium doped siloxane-PMMA hybrid coatings with high anticorrosive performance. RSC Advances. 2015;**5**:15414-15424. DOI: 10.1039/c4ra15974h.

[12] Blaiszik B. J., Kramer S. L. B., Olugebefola S. C., Moore J. S., Sottos N. R., White, S. R. Self-healing polymers and composites. Annual Review of Materials Research. 2010;**40**:179-211. DOI: 10.1146/annurev-matsci-070909-104532.

[13] Fischer H. R., García S. J. Active protective coatings: Sense and heal concepts for organic coatings. In: Hughes A. E., Mol J. M. C., Zheludkevich M. L., Buchheit R. G., editors. Active protective coatings: New-generation coatings for metals. Dordrecht, The Netherlands: Springer Science+Business Media B.V; 2016. 139-156. DOI: 10.1007/978-94-017-7540-3_7.

[14] Hammer P., Schiavetto M. G., dos Santos F. C., Benedetti A. V., Pulcinelli S. H., Santilli C. V. Improvement of the corrosion resistance of polysiloxane hybrid coatings by cerium doping. Journal of Non-Crystalline Solids. 2010;**356**(44-49):2606-2612. DOI: 10.1016/j.jnoncrysol.2010.05.013.

[15] Pepe A., Aparicio M., Ceré S., Durán A. Preparation and characterization of cerium doped silica sol-gel coatings on glass and aluminum substrates. Journal of Non-Crystalline Solids. 2004;**348**:162-171. DOI: 10.1016/j.jnoncrysol.2004.08.141.

[16] Suegama P. H., Sarmento V. H. V., Montemor M. F., Benedetti A. V., De Melo H. G., Aoki I. V., Santilli C. V. Effect of cerium (IV) ions on the anticorrosion properties of siloxane-poly(methyl methacrylate) based film applied on tin coated steel. Electrochimica Acta. 2010;**55**:5100-5109. DOI: 10.1016/j.electacta.2010.04.002.

[17] Montemor M. F., Pinto R., Ferreira M. G. S. Chemical composition and corrosion protection of silane films modified with CeO2 nanoparticles. Electrochimica Acta. 2009;**54**(22):5179-5189. DOI: 10.1016/j.electacta.2009.01.053.

[18] Harb S. V., Pulcinelli S. H., Santilli C. V., Knowles K., Hammer P. A comparative study on graphene oxide and carbon nanotube reinforcement of PMMA-siloxane-silica anticorrosive coatings. ACS Applied Materials & Interfaces. 2016;**8**:16339-16350. DOI: 10.1021/acsami.6b04780.

[19] Harb S. V., dos Santos F. C., Pulcinelli S. H., Santilli C. V., Knowles K., Hammer P. Protective coatings based on PMMA-silica nanocomposites reinforced with carbon nanotubes. In: Berber M. R., Hafez I. H., editors. Carbon nanotubes–current progress of their polymer composites. 1st ed. Rijeka, Croatia: Intech; 2016. 195-225. DOI: 10.5772/62808.

[20] Harb S. V., Cerrutti B. M., Pulcinelli S. H., Santilli C. V., Hammer P. Siloxane-PMMA hybrid anti-corrosion coatings reinforced by lignin. Surface and Coatings Technology. 2015;**275**:9-16. DOI: 10.1016/j.surfcoat.2015.05.002.

[21] Callister W. D., Rethwisch D. G.. Appendix B/properties of selected engineering materials. In: Callister W. D., Rethwisch D. G., editors. Fundamentals of materials science and engineering: An integrated approach. 2012. 4th ed. Hoboken: Wiley. pp. 835-836.

[22] Hammer P., dos Santos F. C., Cerrutti B. M., Pulcinelli S. H., Santilli C. V. Highly corrosion resistant siloxanepolymethyl methacrylate hybrid coatings. Journal of Sol-Gel Science and Technology. 2012;**63**(2):266-274. DOI: 10.1007/s10971-011-2672-8.

[23] Cole K. C., Hechler J. J., Noel D. New approach to modeling the cure kinetics of epoxy amine thermosetting resins. 2. Application to a typical system based on bis[4-(diglycidylamino)phenyl]methane and bis(4-aminophenyl) sulfone. Macromolecules. 1991;**24**(11):3098-3110. DOI: 10.1021/ma00011a012.

[24] Dahmouche K., Carlos L. D., Zea Bermudez V., SA Ferreira R. A., Santilli, C. V., Craievich A. F. Structural modelling of Eu3z-based siloxane–poly(oxyethylene) nanohybrids. Journal of Materials Chemistry. 2011;**11**(12):3249-3257. DOI: 10.1039/B104822H.

[25] Zaioncz S., Dahmouche K., Paranhos C. M., San Gil R. A. S., Soares B. G. Relationships between nanostructure and dynamic-mechanical properties of epoxy network containing PMMA-modified silsesquioxane. eXPRESS Polymer Letters. 2009;**3**(6):340-351. DOI: 10.3144/expresspolymlett.2009.43.

[26] Zadeh M. A., Van Der Zwaag S., Garcia S. J. Adhesion and long-term barrier restoration of intrinsic self-healing hybrid sol-gel coatings. ACS Applied Materials & Interfaces. 2016;**8**(6):4126-4136. DOI: 10.1021/acsami.5b11867.

[27] Díaz I., Chico B., De La Fuente D., Simancas J., Vega J. M., Morcillo M. Corrosion resistance of new epoxy–siloxane hybrid coatings. A laboratory study. Progress in Organic Coatings. 2010;**69**:278-286. DOI: 10.1016/j.porgcoat.2010.06.007.

[28] Mallakpour S., Zadehnazari A. Preparation of dopamine-functionalized multi-wall carbon nanotube/poly(amide-imide) composites and their thermal and mechanical properties. New Carbon Materials. 2016;**31**(1):18-30. DOI: 10.1016/S1872-5805(16)60001-X.

[29] Khun N. W., Troconis B. C. R., Frankel G. S. Effects of carbon nanotube content on adhesion strength and wear and corrosion resistance of epoxy composite coatings on AA2024-T3. Progress in Organic Coatings. 2014;**77**(1):72-80. DOI: 10.1016/j.porgcoat.2013.08.003.

[30] Hammer P., dos Santos F. C., Cerrutti B. M., Pulcinelli S. H., Santilli C. V. Carbon nanotube-reinforced siloxane-PMMA hybrid coatings with high corrosion resistance. Progress in Organic Coatings. 2013;**76**(4):601-608. DOI: 10.1016/j.porgcoat.2012.11.015.

[31] Mosa J., Navarro N. C. R., Aparicio M. Active corrosion inhibition of mild steel by environmentally-friendly Ce-doped organic-inorganic sol-gel coatings. RSC Advances. 2016;**6**:39577-39586. DOI: 10.1039/c5ra26094a.

[32] López D. D. A., Crespo M. A. D., Huerta A. M. T., Vela A. F., Adame J. A., Rosales H. D. Analysis of degradation process during the incorporation of ZrO2:SiO2 ceramic nanostructures into polyurethane coatings for the corrosion protection of carbon steel. Journal of Materials Science. 2013;**48**:1067-1084. DOI: 10.1007/s10853-012-6839-7.

[33] Brusciotti F., Snihirova D. V., Xue H., Montemor M. F., Lamaka S. V., Ferreira M. G. S. Hybrid epoxy–silane coatings for improved corrosion protection of Mg alloy. Corrosion Science. 2013;**67**:82-90. DOI: 10.1016/j.corsci.2012.10.013.

[34] Qiao Y., Li W., Wang G., Zhang X., Cao N. Application of ordered mesoporous silica nanocontainers in an anticorrosive epoxy coating on a magnesium alloy surface. RSC Advances. 2015;**5**:47778-47787. DOI: 10.1039/c5ra05266a.

[35] Ammar S. H., Ramesh K., Vengadaesvaran B., Ramesh S., Arof A. K. Amelioration of anticorrosion and hydrophobic properties of epoxy/PDMS composite coatings containing nano ZnO particles. Progress in Organic Coatings. 2016;**92**:54-65. DOI: 10.1016/j.porgcoat.2015.12.007.

[36] Yuan X., Yue Z. F., Chen X., Wen S. F., Li L., Feng T. The protective and adhesion properties of silicone-epoxy hybrid coatings on 2024 Al-alloy with a silane film as pretreatment. Corrosion Science. 2016;**104**:84-97. DOI: 10.1016/j.corsci.2015.11.035.

[37] Lamaka S. V., Xue H. B., Meis N. N. A. H., Esteves A. C. C., Ferreira M. G. S. Fault-tolerant hybrid epoxy-silane coating for corrosion protection of magnesium alloy AZ31. Progress in Organic Coatings. 2015;**80**:98-105. DOI: 10.1016/j.porgcoat.2014.11.024.

[38] Kozhukharov S., Kozhukharov V., Schem M., Aslan M., Wittmar M., Wittmar A., Veith M. Protective ability of hybrid nano-composite coatings with cerium sulphate as inhibitor against corrosion of AA2024 aluminium alloy. Progress in Organic Coatings. 2012;**73**(1):95-103. DOI: 10.1016/j.porgcoat.2011.09.005.

[39] Khelifa F., Druart M. E., Habibi Y., Bénard F., Leclere P., Olivier M., Dubois P. Sol-gel incorporation of silica nanofillers for tuning the anti-corrosion protection of acrylate-based coatings. Progress in Organic Coatings. 2013;**76**:900-911. DOI: 10.1016/j.porgcoat.2013.02.005.

[40] Ammar S. H., Ramesh K., Vengadaesvaran B., Ramesh S., Arof A. K. Formulation and characterization of hybrid polymeric/ZnO nanocomposite coatings with remarkable anti-corrosion and hydrophobic characteristics. Journal of Coatings Technology and Research. 2016;**13**(5):921-930. DOI: 10.1007/s11998-016-9799-z.

[41] Mostafaei A., Nasirpouri F. Epoxy/polyaniline–ZnO nanorods hybrid nanocomposite coatings: Synthesis, characterization and corrosion protection performance of conducting paints. Progress in Organic Coatings. 2014;**77**:146-159. DOI: 10.1016/j.porgcoat.2013.08.015.

[42] Zomorodian A., Garcia M. P., Moura e Silva T., Fernandes J. C. S., Fernandes M. H., Montemor M. F. Corrosion resistance of a composite polymeric coating applied on biodegradable AZ31 magnesium alloy. Acta Biomaterialia. 2013;**9**:8660-8670. DOI: 10.1016/j.actbio.2013.02.036.

[43] Zheludkevich M. L., Poznyak S. K.,Rodrigues, L. M., Raps D., Hack T., Dick L. F., Nunes T., Ferreira M. G. S. Active protection coatings with layered double hydroxide nanocontainers of corrosion inhibitor. Corrosion Science. 2010;**52**:602-611. DOI: 10.1016/j.corsci.2009.10.020.

[44] Snihirova D., Liphardt L., Grundmeier G., Montemor F. Electrochemical study of the corrosion inhibition ability of "smart" coatings applied on AA2024. Journal of Solid State Electrochemistry. 2013;**17**:2183-2192. DOI: 10.1007/s10008-013-2078-3.

[45] Snihirova D., Lamaka S. V., Montemor M. F. "SMART" protective ability of water based epoxy coatings loaded with CaCO3 microbeads impregnated with corrosion inhibitors applied on AA2024 substrates. Electrochimica Acta. 2012;**83**:439-447. DOI: 10.1016/j.electacta.2012.07.102.

[46] Okafor P. A., Beemat J. S., Iroh J. O. Thermomechanical and corrosion inhibition properties of graphene/epoxy ester–siloxane–urea hybrid polymer nanocomposites. Progress in Organic Coatings. 2015;**88**:237-244. DOI: 10.1016/j.porgcoat.2015.07.00.